Biophysical and Pharmacological Characteristics of Native Two-Pore Domain TASK Channels in Rat Adrenal Glomerulosa Cells

David P. Lotshaw

Department of Biological Sciences, Northern Illinois University, DeKalb, Illinois 60115

Abstract. Multiple genes of the TASK subfamily of two-pore domain K^+ channels are reported to be expressed in rat glomerulosa cells. To determine which TASK isoforms contribute to native leak channels controlling resting membrane potential, patch-clamp studies were performed to identify biophysical and pharmacological characteristics of macroscopic and unitary K^+ currents diagnostic of recombinant TASK channel isoforms. Results indicate K^+ conductance (gK^+) is mediated almost exclusively by a weakly voltage-dependent (leak) K^+ channel closely resembling TASK-3. Leak channels exhibited a unitary conductance approximating that expected for TASK-3 under the recording conditions employed, brief mean open times and a voltage-dependent open probability. Extracellular H^+ induced voltage-independent inhibition of gK^+, exhibiting an IC_{50} of 56 nM (pH 7.25) and a Hill coefficient of 0.75. Protons inhibited leak channel open probability (P_o) by promoting a long-lived closed state ($\tau > 500$ ms). Extracellular Zn^{2+} mimicked the effects of H^+; inhibition of gK^+ exhibited an IC_{50} of 41 μM with a Hill coefficient of 1.26, inhibiting channel gating by promoting a long-lived closed state. Ruthenium red (5 μM) inhibited gK^+ by 75.6% at 0 mV. Extracellular Mg^{2+} induced voltage-dependent block of gK^+, inhibiting unitary current amplitude without affecting mean open time. Bupivacaine induced voltage-dependent block of gK^+, exhibiting IC_{50} values of 116 μM at −100 mV and 28 μM at 40 mV with Hill coefficients of 1 at both potentials. Halothane induced a voltage-independent stimulation of gK^+ primarily by decreasing the leak channel closed-state dwell time.

Introduction

Leak K^+ channels responsible for the resting membrane potential and membrane excitability in a variety of cell types eluded molecular characterization until discovery of the two-pore domain family of K^+ channels. These channels, named for their novel structural arrangement of two-pore domains responsible for K^+ selectivity within a single polypeptide, were initially identified in yeast and subsequently in invertebrates and mammals (Ketchum et al., 1995; *for reviews, see* Lesage & Lazdunski, 2000; Goldstein et al., 2001; Bayliss, Sirois & Talley, 2003). Mammalian gene homologues identified to date encode a polypeptide possessing two pore domains and four putative transmembrane domains. The mammalian gene family is divided into six subfamilies (Plant, Rajan & Goldstein, 2005). The TASK (TWIK-related acid-sensitive K^+ channel) subfamily includes three members: TASK-1, TASK-3 and TASK-5 or KCNK3, KCNK9 and KCNK15, respectively, in accordance with Human Genome Organization nomenclature. Two-pore domain K^+ channels are thought to function as dimers, and within the TASK subfamily, evidence for functional TASK-1/TASK-3 heteromers has been obtained from heterologous expression of recombinant genes (Czirjak & Enyedi, 2002b; Karschin et al., 2001; Lauritzen et al., 2003; Clarke et al., 2004) and from native cells (Kang et al., 2003; Berg et al., 2004).

Weakly voltage-dependent leak K^+ channels set the resting membrane potential and control membrane excitability in adrenal glomerulosa (AG) cells

---

Correspondence to: David P. Lotshaw; email: dlotshaw@niu.edu

(Lotshaw, 1997a, 2001). Leak K^+ channel regulation is a fundamental component of the cellular mechanisms mediating regulation of aldosterone secretion (Spät & Hunyady, 2004), and in rats, AG cell K^+ conductance (gK^+) is mediated, at least in part, by members of the pH-sensitive TASK channel subfamily (Czirjak et al., 2000; Czirjak & Enyedi, 2002a). Interestingly, TREK-1 channels are reported to dominate the gK^+ of bovine AG cells and TASK-3 expression is undetectable in these cells (Enyeart, Danthi & Enyeart, 2004). The protein subunit composition of rat AG cell TASK channels is unresolved. TASK mRNA expression has been extensively mapped at the tissue and organ levels (Medhurst et al., 2001; Talley et al., 2001; Karschin et al., 2001). Like several organs and brain regions, rat adrenal cortex expresses multiple TASK genes, including TASK-1 (Czirjak et al., 2000) and TASK-3 (Czirjak & Enyedi, 2002a); human adrenal cortex also, expresses TASK-5 (Kim & Gnatenco, 2001). Unlike TASK-1 and TASK-3, TASK-5 expression in *Xenopus* oocytes, COS-7 or HEK-293 cells failed to elicit plasma membrane K^+ currents (Ashmole, Goodwin & Stanfield, 2001; Karschin et al., 2001; Kim & Gnatenco, 2001). Furthermore, coexpression of TASK-5 and TASK-1 or TASK-3 failed to modify current expression relative to expression of TASK-1 or TASK-3 alone. Surface expression of TASK-5 was reported in HEK cells (Ashmole et al., 2001) but not in *Xenopus* oocytes (Karschin et al., 2001). Thus, it remains to be determined whether TASK-5 can form heteromers with other TASK isoforms, whether TASK-5 functions intracellularly or whether plasma membrane channels are silenced by a mechanism such as the sumoylation process described for TWIK-1 (Rajan et al., 2005).

In principle, native K^+ currents mediated by homomeric TASK-1 or TASK-3 and heteromeric TASK-1/TASK-3 channels can be distinguished on the basis of biophysical and pharmacological criteria such as sensitivity to extracellular pH, single-channel conductance and inhibition by ruthenium red or Zn^{2+}. Within this subfamily, cloned TASK-1 channels are the most sensitive to H^+ inhibition, exhibiting a 50% inhibitory concentration (IC_{50}) near pH 7.3 (Duprat et al., 1997; Lopes et al., 2000; Talley et al., 2000). TASK-3 channels are substantially less sensitive, exhibiting an IC_{50} near pH 6.6 (Kim, Bang & Kim, 2000; Rajan et al., 2000; Meadows & Randall, 2001); heteromeric TASK-1/TASK-3 channels exhibit an intermediate sensitivity (Czirjak & Enyedi, 2002b; Berg et al., 2004). In symmetric 100–150 mM K^+ solutions, cloned TASK-1 channels exhibit inward and outward unitary conductances of approximately 14 pS and 10 pS, respectively (Kim, Bang & Kim, 1999; Lopes et al., 2000; Han et al., 2002), whereas TASK-3 conductance nearly doubles these values to approximately 30 pS and 17 pS,

respectively (Kim et al., 2000; Rajan et al., 2000; Han et al., 2002). Although heteromeric TASK-1/TASK-3 conductance is similar to that of TASK-3 (Kang et al., 2003), TASK-3 may be distinguished from the heteromer by its sensitivity to ruthenium red (Czirjak & Enyedi, 2002b; Kang et al., 2003) and Zn^{2+} (Clarke et al., 2004). These criteria, and others, have been employed to characterize native channels mediating TASK-like currents in cells reported to express multiple TASK genes (Han et al., 2002; Kang et al., 2003; Berg et al., 2004; Clarke et al., 2004; Williams & Buckler, 2004). In practice, however, native channel identification based on cloned channel properties should proceed cautiously as native channels may undergo modifications that substantially change their properties (Bockenhauer, Zilberberg & Goldstein, 2001; Rajan et al., 2005). Native channel characterization is typically performed on heterogenous cell populations under conditions that may downregulate expression or induce novel channel modifications as well as expression of channels not present *in vivo*.

Based on mRNA expression and K^+ current inhibition by ruthenium red, TASK-like K^+ currents in rat AG cells are postulated to be mediated predominantly by TASK-3 channels, with some contribution from TASK-1 channels (Czirjak & Enyedi, 2002a). Several other K^+ channel classes have been described in cultured rat, bovine and human AG cells; the extent to which these channels represent cell culture artifacts or functional components within a heterogenous glomerulosa cell population has not been established (*for review, see* Spät & Hunyady, 2004). Nevertheless, leak K^+ channels appear to predominate control of the resting membrane potential (Lotshaw, 1997a, 1997b; Enyeart et al., 2004). In rat AG cells, the weakly voltage-dependent leak channels represent obvious candidates for native TASK channels. The present study was undertaken to measure the biophysical and pharmacological properties of rat AG cell macroscopic and single leak channel K^+ currents for comparison with those reported for cloned TASK channel isoforms and to determine the proportion of gK^+ mediated by TASK-like channels. Our results indicate that effectively all the resting gK^+ and as much as 90% of depolarization-activated gK^+ is mediated by a single homogenous TASK channel population in the AG cells examined. The characteristics of this channel most closely resemble TASK-3; however, the pH sensitivity of this native channel was substantially greater than that of recombinant TASK-3. Thus, either native channels had undergone posttranslational or other modifications affecting pH sensitivity or undetectable contributions from other TASK isoforms, such as TASK-1/TASK-3 heteromers, were sufficient to shift pH sensitivity of the macroscopic current.

Methods

AG Cell Isolation and Culture

All animal protocols used in this study were approved by the Northern Illinois University Institutional Animal Care and Use Committee in accordance with all regulations and recommendations of the Office of Laboratory Animal Welfare, National Institutes of Health. Primary cultures of rat AG cells were prepared as previously described (Lotshaw, 1997a) using female Sprague-Dawley rats weighing 150–200 g (Harlan, Indianapolis, IN). Briefly, animals were anesthetized by CO_2 inhalation and subsequently killed by decapitation prior to adrenal gland dissection. Glomerulosa cells were isolated using a collagenase (type IV) dispersion method; isolated cells were plated at low density (fewer than 10^5 cells/ml) on fibronectin-coated glass coverslip chips and maintained in culture medium at 37°C in a humidified atmosphere of 5% CO_2-95% air. Culture medium consisted of a mixture of Ham's F-12 and Dulbecco's modified Eagle's medium (1:1 by volume) supplemented to contain 2% fetal bovine serum, 8% horse serum, 0.1 mm ascorbic acid, 10 µg/ml insulin, 5.5 µg/ml transferrin, 6.7 ng/ml selenite, 50 U/ml penicillin G, 50 µg/ml streptomycin and 1 µM tocopherol. Culture media, insulin-transferrin-selenium media supplement, fetal bovine sera and horse sera were obtained from Life Technologies (Grand Island, NY), collagenase was from Worthington Biochemical (Freehold, NJ), and all other reagents were from Sigma (St. Louis, MO).

Patch Clamp

Whole-cell and cell-attached patch-clamp recordings were performed at room temperature on cells maintained in culture for 12–48 h. Glass coverslip chips containing adherent cells were transferred from culture dishes to a recording chamber (0.5 ml volume) and continuously superfused with gravity-driven saline at a rate of 1 ml / min^{-1}. Single AG cells were identified by visual appearance under phase contrast microscopy. Solution changes and drugs were delivered to the recording chamber by switching saline input lines; the lag time for solution changes or drug delivery was approximately 30 s. Rapid solution changes (less than 100 ms) were achieved with a switch-controlled, gravity-driven perfusion pipette positioned adjacent to the recorded cell.

Patch pipettes were fabricated from Corning (Corning, NY) 7052 capillary glass. Pipettes were pulled to have resistances of 2–3 MΩ (whole-cell) or 6–10 MΩ (cell-attached) when filled with saline. Pipette tips were coated with Sylgard (Dow-Corning, Midland, MI) to within 100 µm of the tip. Whole-cell pipette saline contained (in mm): 120 KCl, 2 MgCl$_2$, 10 4-(2-hydroxyethyl)-1-piperazineethanesulfonic acid (HEPES), 10 ethyleneglycoltetraacetic acid (EGTA), 4 magnesium adenosine triphosphate (MgATP) and 0.2 guanosine triphosphate (GTP), pH adjusted to 7.2 with KOH. Cell-attached pipette saline routinely contained (in mm) 20 KCl, 130 NaCl, 1.2 MgCl$_2$ and 10 HEPES, pH adjusted with NaOH. Cell-attached pipette saline was formulated to give a K$^+$ equilibrium potential (E_K) near −50 mV in order to distinguish unitary K$^+$ currents from nonselective cation currents whose reversal potential is near 0 mV under the recording conditions employed. In order to ensure pH buffering in the cell-attached pipette saline at pH extremes (pH 6.5 and 8.5), experiments were repeated substituting a buffer mixture for 10 mm HEPES (in mm): 10 Gly-Gly, 10 HEPES and 10 BIS-TRIS, pH adjusted to 6.5 or 8.5 with HCl or NaOH (NaCl concentration was lowered to maintain osmolarity).

The standard extracellular saline contained (in mm) 140 NaCl, 4 KCl, 1.25 CaCl$_2$, 1.2 MgCl$_2$, 4.2 NaHCO$_3$, 10 HEPES and 5.5 glucose, pH adjusted to 7.4 with NaOH. For measurement of macroscopic K$^+$ current (I_K), this solution was modified by increasing K$^+$ and decreasing Ca^{2+} concentrations (lowering NaCl to maintain osmolarity) in order to increase inward K$^+$ current and reduce voltage-dependent Ca^{2+} current (in mm): 138 NaCl, 10 KCl, 0.1 CaCl$_2$, 1.2 MgCl$_2$, 5.5 glucose and 10 HEPES, pH adjusted with NaOH. In the whole-cell configuration, rundown of L-type Ca^{2+} channels further contributed to isolation of I_K (Lotshaw, 2001). To ensure pH buffering of the extracellular saline at the extremes of pH utilized, experiments were repeated substituting a buffer mixture for 10 mm HEPES in the bath saline (in mm): 10 Gly-Gly, 10 HEPES and 10 BIS-TRIS, with pH adjusted to its final value by addition of NaOH or HCl (NaCl concentration was lowered to maintain osmolarity). In cell-attached patch clamp, the resting membrane potential was set to 0 mV by bathing the cell in high-K$^+$ saline (in mm): 145 KCl, 4.2 NaHCO$_3$, 1 EGTA, 2 MgCl$_2$, 10 HEPES and 5 glucose, pH adjusted to 7.4 with NaOH.

Membrane currents were measured with an Axopatch 200A amplifier (Axon Instruments, Foster City, CA). Macroscopic and unitary currents were low pass-filtered at 10 and 2 kHz (−3 dB), respectively, using a four-pole Bessel filter and digitized at 10 or 20 kHz. Whole-cell recordings employed capacitance and series resistance compensation (≥ 75%). Acquired data were stored on a computer for later analysis. Membrane voltages are expressed without correction for liquid junction potentials (< 3 mV).

Data Analysis

Current records were analyzed using pCLAMP 6.0 software (Axon Instruments). Under the recording conditions employed, macroscopic current was previously shown to be predominantly mediated by K$^+$ channels (Lotshaw, 1997a). Potassium current amplitude was measured following subtraction of ohmic leakage current. Ohmic leak current was represented as current which is not blocked at an extracellular pH of 5.5. This remnant current was linear over a voltage range of −140 to 20 mV, reversing near 0 mV. It was not further diminished over this voltage range by addition of extracellular K$^+$ channel blockers. The amplitude of leak current at pH 5.5 was similar to that obtained in Cs$^+$-loaded cells (Lotshaw, 1997a, 2001). For potentials above 20 mV, ohmic leak was determined by linear extrapolation of the current-voltage relationship obtained below 20 mV. Macroscopic gK$^+$ was calculated as chord conductance determined from K$^+$ current amplitude measured at the end of each voltage command and its reversal potential. Current relaxations were fitted using the simplex least squares minimization algorithm to estimate the number of kinetic components present and their time constants. Relaxation amplitudes were determined by extrapolation of the fit to the onset of the voltage command. Drug and H$^+$ dose-response parameters were determined using a Marquardt-Levenberg least squares algorithm to fit the normalized data to a logistic equation of the following form:

$$I = [1 + (\mathrm{IC}_{50}/B)^{-n}]^{-1} \qquad (1)$$

where I represents the normalized current or conductance, IC$_{50}$ the blocker concentration at which 50% inhibition occurred, B the blocker concentration and n the Hill coefficient. The voltage dependence of inhibitor effects was modeled after Woodhull (1973):

$$K_d(V) = K_d(0)\exp(-z\delta\,VF/RT) \qquad (2)$$

where $K_d(0)$ and $K_d(V)$ represent the apparent dissociation constant at 0 mV and a specified potential, respectively; z the electrical charge of the inhibitor; δ the proportion of the electric field traversed by the inhibitor; V the membrane potential, F is Faraday's constant, R the gas constant, and T is temperature

Single-channel current records were further low pass-filtered at 1 kHz using a digital gaussian filter prior to analysis. Channel openings and closings were interactively detected using a threshold set to 50% of the predominant open channel current level. Unitary

current amplitudes were obtained from amplitude histograms of single channel openings fitted to a gaussian distribution. Unitary conductance was expressed as slope conductance. Mean open and closed times were determined from exponential fits of open and closed dwell time distributions using the method of maximum likelihood. The dead time of the recording system was approximately 0.15 ms at a cut-off filter setting of 2 kHz. Mean open time determinations were not adjusted for missed events.

Statistical analyses were performed using Student's t-test and Student's t-test for paired comparisons.

Results

Biophysical Characteristics and Effect of Extracellular pH on Macroscopic K^+ Current

Whole-cell patch-clamp experiments revealed that macroscopic K^+ current (I_K) is profoundly sensitive to extracellular pH (Fig. 1). Both inhibition and recovery of I_K in response to pH changes occurred within seconds, indicating these effects were not due to changes in intracellular pH subsequent to extracellular pH changes. Current responses to hyperpolarizing and depolarizing voltage commands are shown at four pH values (Fig. 1A). As previously described (Lotshaw, 1997a), quasi-steady-state I_K exhibited strong outward rectification. Depolarizing commands from a holding potential of −80 mV induced rapidly activating outward current composed of two kinetic components: an apparently instantaneous component and, at voltages above −40 mV, a time-dependent component. At command potentials equal to or greater than 60 mV, I_K occasionally exhibited partial inactivation (not readily apparent in the cell shown). The I_K response to hyperpolarizing voltage commands (and upon repolarization) also exhibited an apparently instantaneous jump followed by partial deactivation (not readily visible at the scale shown). Increasing external pH from 7.5 to 10.0 substantially increased both instantaneous and time-dependent components of I_K, whereas decreasing pH below 7.5 inhibited both components. Current appeared to be maximal at pH 9.5; however, an irreversible leak current often developed when cells were exposed to pH 10 saline. The reversal potential (E_{rev}) of the pH-sensitive current, measured at the end of each voltage command, was -63.1 ± 2.4 mV (mean ± standard deviation [SD]) ($n = 10$), very close to the expected E_K of −64 mV under the recording conditions employed. Proton inhibition of gK^+ was voltage-independent (Fig. 1B); no significant differences were observed in the pH sensitivity of the quasi-steady-state gK^+ obtained at −100 and 40 mV. The best fit of the pooled data to the Hill equation (equation 1) yielded an IC_{50} of 56 nM H^+ (pH 7.25) and a Hill coefficient of 0.75.

We previously hypothesized that at least two K^+ channel classes mediate gK^+: a weakly voltage-dependent leak channel active at rest and a more
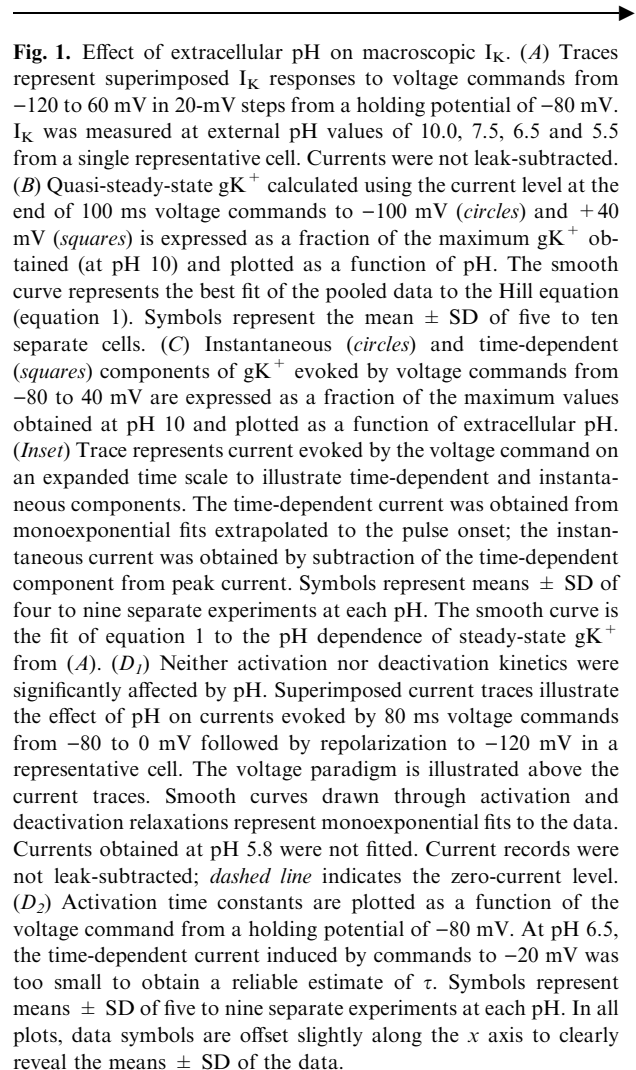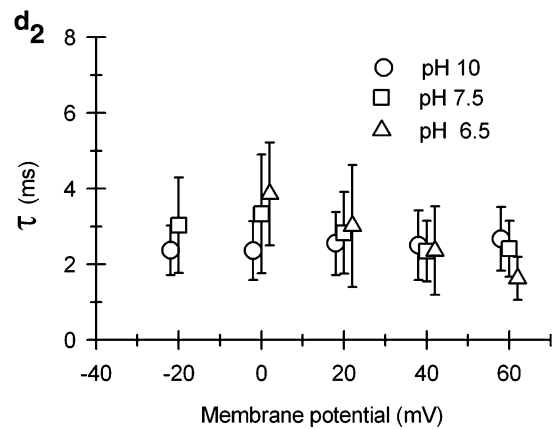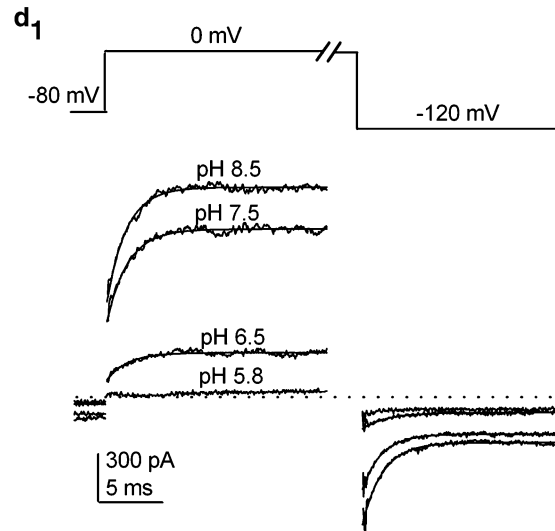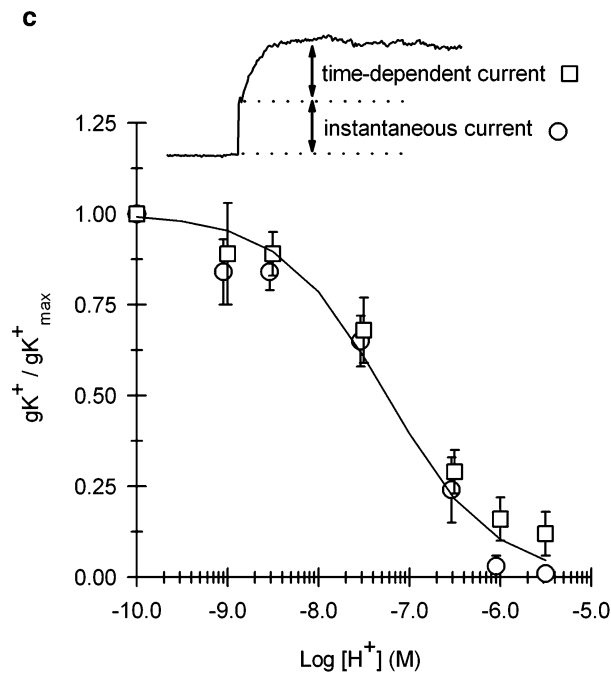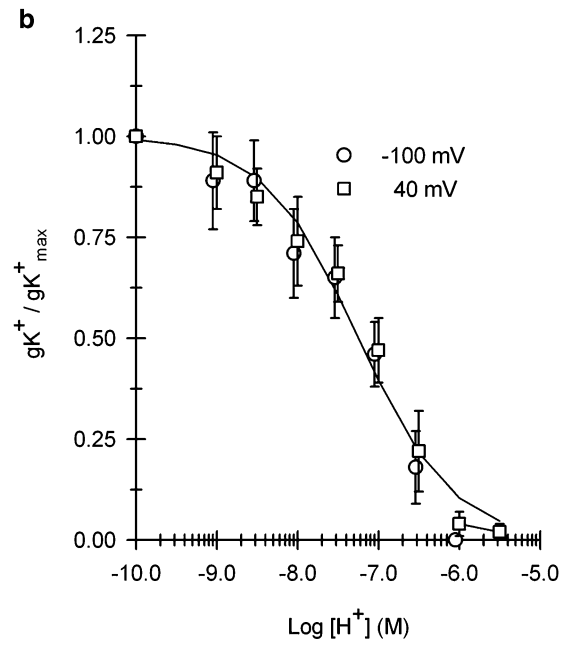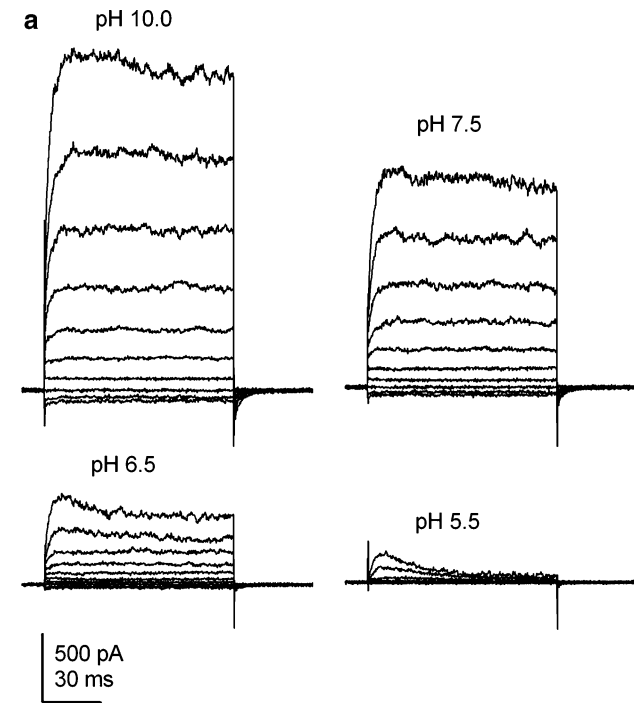
Fig. 1. Effect of extracellular pH on macroscopic I_K. (A) Traces represent superimposed I_K responses to voltage commands from −120 to 60 mV in 20-mV steps from a holding potential of −80 mV. I_K was measured at external pH values of 10.0, 7.5, 6.5 and 5.5 from a single representative cell. Currents were not leak-subtracted. (B) Quasi-steady-state gK^+ calculated using the current level at the end of 100 ms voltage commands to −100 mV (circles) and +40 mV (squares) is expressed as a fraction of the maximum gK^+ obtained (at pH 10) and plotted as a function of pH. The smooth curve represents the best fit of the pooled data to the Hill equation (equation 1). Symbols represent the mean ± SD of five to ten separate cells. (C) Instantaneous (circles) and time-dependent (squares) components of gK^+ evoked by voltage commands from −80 to 40 mV are expressed as a fraction of the maximum values obtained at pH 10 and plotted as a function of extracellular pH. (Inset) Trace represents current evoked by the voltage command on an expanded time scale to illustrate time-dependent and instantaneous components. The time-dependent current was obtained from monoexponential fits extrapolated to the pulse onset; the instantaneous current was obtained by subtraction of the time-dependent component from peak current. Symbols represent means ± SD of four to nine separate experiments at each pH. The smooth curve is the fit of equation 1 to the pH dependence of steady-state gK^+ from (A). (D_1) Neither activation nor deactivation kinetics were significantly affected by pH. Superimposed current traces illustrate the effect of pH on currents evoked by 80 ms voltage commands from −80 to 0 mV followed by repolarization to −120 mV in a representative cell. The voltage paradigm is illustrated above the current traces. Smooth curves drawn through activation and deactivation relaxations represent monoexponential fits to the data. Currents obtained at pH 5.8 were not fitted. Current records were not leak-subtracted; dashed line indicates the zero-current level. (D_2) Activation time constants are plotted as a function of the voltage command from a holding potential of −80 mV. At pH 6.5, the time-dependent current induced by commands to −20 mV was too small to obtain a reliable estimate of τ. Symbols represent means ± SD of five to nine separate experiments at each pH. In all plots, data symbols are offset slightly along the x axis to clearly reveal the means ± SD of the data.

strongly voltage-dependent channel activated by depolarization above −50 mV (Lotshaw, 1997a). If the instantaneous and time-dependent components of depolarization-activated current are mediated by different channel classes, then we might expect these components to differ in pH sensitivity. This, however, was not observed except for a small proportion of the time-dependent component (Fig. 1C). Separation of depolarization-activated I_K into instantaneous and time-dependent components revealed similar pH sensitivities except below pH 6.5. Instantaneous current was abolished at pH 6.0, whereas approximately 10% of the time-dependent current remained. This pH-insensitive current decayed during the pulse such that its contribution to quasi-steady-state gK^+ was small (see Fig. 1A, pH 5.5). As illustrated in the macroscopic current traces (Fig. 1A, pH 5.5), this pH-insensitive component was observed only in response to depolarizing commands to 20 mV or greater. The large voltage dependence for activation of this component suggests it was not mediated by

a pH 10.0

pH 7.5

pH 6.5

pH 5.5

500 pA
30 ms

b

1.25

1.00

0.75

gK^+ / gK^+_{max}

0.50

0.25

0.00

○ −100 mV
□ 40 mV

−10.0   −9.0   −8.0   −7.0   −6.0   −5.0

Log $[H^+]$ (M)

c

time-dependent current □
instantaneous current ○

1.25

1.00

0.75

gK^+ / gK^+_{max}

0.50

0.25

0.00

−10.0   −9.0   −8.0   −7.0   −6.0   −5.0

Log $[H^+]$ (M)

d₁

0 mV

−80 mV

−120 mV

pH 8.5
pH 7.5

pH 6.5
pH 5.8

300 pA
5 ms

d₂

8

6

τ (ms)

4

2

0

○ pH 10
□ pH 7.5
△ pH 6.5

−40   −20   0   20   40   60

Membrane potential (mV)

TASK channels. This conclusion was further supported by the observation that halothane stimulation of macroscopic current was completely blocked by lowering external pH to 6.0 (*data not shown*).

Studies of recombinant TASK-1 and TASK-3 channels have reported that decreasing extracellular pH inhibits macroscopic current amplitude without affecting voltage-dependent activation kinetics (Lopes et al., 2000; Rajan et al., 2000; Meadows & Randall, 2001). Similarly, neither activation nor deactivation kinetics of I_K were affected by extracellular pH (Fig. $1D_1$). Activation and deactivation (measured upon repolarization to −120 mV) kinetics were well described by monoexponential functions. The activation time constant was independent of pulse potential, although it appeared to exhibit weak voltage dependence at pH 6.5 (Fig. $1D_2$). This apparent voltage dependence of activation at pH 6.5 may be attributable to the proportionally greater contribution of pH-insensitive channels at low pH and increasing depolarization. Thus, activation of pH-insensitive channels is expected to be slightly faster than that of pH-sensitive channels.

Leak Channels Mediate Voltage-Dependent gK^+

The similarity in pH sensitivity of the instantaneous and time-dependent components of I_K suggests both are mediated predominantly by a single channel type. This hypothesis is further supported by a Hill coefficient near 1 for H^+ inhibition of I_K. The primary candidate for mediating both components of I_K is the weakly voltage-dependent (leak) K^+ channel previously observed to predominate cell-attached patches (Lotshaw, 1997a, 1997b). If leak channels mediate the voltage-dependent component of I_K, then they must exhibit activation kinetics identical to those of the macroscopic current. As shown in Figure 2, the ensemble average of unitary leak channel current responses to large depolarizing commands exhibited both instantaneous and time-dependent kinetic components. In the example shown, the time-dependent component was described well by a single exponential function exhibiting a time constant of 3.5 ms; the mean (± SD) of six different patches was 3.3 ± 1.3 ms. Thus, leak channel activation kinetics are consistent with the hypothesis that this channel mediates the pH-sensitive component of depolarization-activated I_K. In our previous experiments on leak channel activation (Lotshaw, 1997a), smaller pulse potentials were utilized and voltage-dependent activation was not measurable from the ensemble averages. Larger depolarizations (to 50 mV) utilized in the present study were required in order to obtain measurable activation kinetics from patches containing sufficiently few channels that unitary currents were well resolved.

Additional support for the role of leak channels in mediating the voltage-dependent outward K^+ current can be found in the similarity between the voltage dependence of the time-dependent component of I_K and leak channel gating. The time-depen-

dent component of I_K is just detectable in voltage commands to −40 mV and increases as a proportion of gK^+ with increasing depolarization (*analysis not shown, see* Fig. 1A). Leak channel open probability and mean open time increase sharply at potentials above −20 mV (Fig. 3B, C). Leak channels also exhibited a corresponding voltage-dependent decrease in the time constant of the predominant kinetic component of the closed-time distribution (*data not shown, see* Fig. 3F). As discussed below, only multichannel cell-attached patches were obtained in the present study and closed-state dwell times could not be measured directly.

Effect of Extracellular pH on Single Leak K^+ Channels

The effect of extracellular pH on unitary leak channel currents was examined in cell-attached patches by comparing currents recorded from separate patches at pH 6.5 and 8.5, a pH difference expected to select for TASK-3 over TASK-1 at low pH. The results of this comparison indicated a single leak channel type predominates the cell-attached patches and that H^+ inhibition of leak channels is attributable to induction of a long-lived closed state. Firstly, pH did not affect unitary current amplitude (Fig. 3A), indicating that a single type of leak channel is predominantly expressed. Under the ionic conditions employed (20 mM K^+ and 1.2 mM Mg^{2+} pipette saline), channels exhibited nearly linear outward and inward slope conductances of 12 and 8 pS, respectively, and a reversal potential of -52 mV at both pH 8.5 and 6.5. These data were similar to results obtained previously at pH 7.4 (Lotshaw, 1997a). Leak channel conductance most closely approximated that expected of TASK-3 or TASK-1/TASK-3 heteromers under these ionic conditions. If both homomeric TASK-1 and TASK-3 (or heteromeric TASK-1/TASK-3) isoforms contributed to gK^+, then at pH 6.5 TASK-1 would have been expected to be inhibited relative to TASK-3 and mean unitary current amplitude increased due to a proportionately greater contribution from the larger TASK-3 currents.

Secondly, although cell-attached patches always contained either multiple active channels or no channels, precluding direct analysis of closed-state dwell times, the conclusion that protonation induced a long-lived closed state was supported by several measures. Single-channel mean open times (τ_o) were similar at both pH 6.5 and 8.5 (Fig. 3B). Although τ_o was shorter at pH 8.5 than pH 6.5 at the most negative potentials, this difference was not statistically significant. At more positive potentials, shorter τ_o values at pH 8.5 were biased by higher NP_o values (the number of available channels [N] multiplied by the single-channel open probability [P_o]) obtained at pH 8.5. High NP_o values biased τ_o determinations by
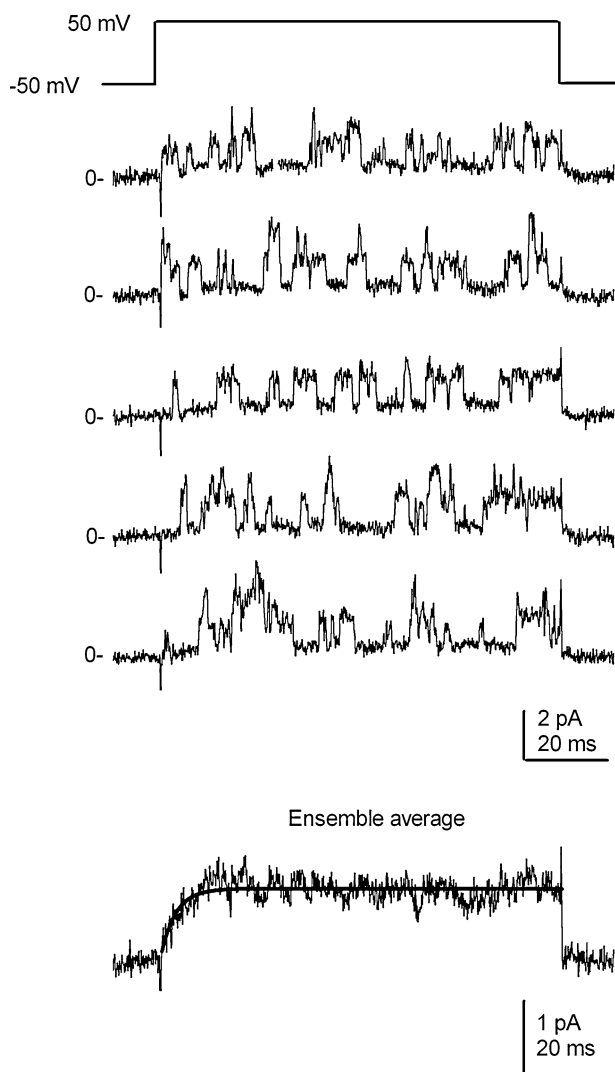
Fig. 2. Leak K^+ channel activation kinetics. Ensemble average of unitary leak channel currents evoked by repeated depolarizing commands in a cell-attached patch at pH 6.5. The voltage paradigm consisted of 0.5-Hz 100-ms pulses from a holding potential of -50 to $+50$ mV (*top trace*). Subsequent traces illustrate five successive repetitions of leak- and capacitance-subtracted current responses to the voltage command. Current records were low pass-filtered at 2,000 Hz. The 0 at the left of each trace indicates the zero-current level. The *lowermost trace* represents the ensemble average of 30 successive responses. The smooth curve drawn through the ensemble average represents the best fit of a mono-exponential function exhibiting a time constant of 3.5 ms. The patch contained at least four channels, although a maximum of only three simultaneously open channels can be seen in the traces shown.

increasing the likelihood that long open time events included multiple channel openings and, therefore, were excluded from analysis. At hyperpolarized potentials, multiple channel openings were infrequent, even at pH 8.5, and their exclusion was not expected to bias τ_o. The absence of significant pH effects on unitary current amplitude or mean open

time indicated that H^+ inhibited leak channels by affecting closed-state dwell times. If so, then protonation must act by reducing channel open probability as previously suggested (Kim et al., 1999, 2000; Han et al., 2002). The effect of pH on leak channel open probability, measured as NP_o, was compared over a range of voltages for data collected from patches that appeared to contain similar numbers of active channels (Fig. 3C). The number of active channels in each patch was estimated as the maximum number of simultaneously open channels at depolarized potentials. At pH 8.5, NP_o was nearly threefold greater than at pH 6.5 over the entire range of voltages. The validity of comparing NP_o values from different patches rests on the assumption that patches contained similar numbers of active channels. However, estimation of channel number is problematic when P_o is low (Horn, 1991), more so if gating is nonstationary. Nonstationary gating was often observed at pH 6.5, as illustrated in the comparison of representative recordings of continuous channel activity from patches at pH 6.5 and 8.5 (Fig. 3D). This figure compares patches in which the maximum number of simultaneously open channels was four. At pH 6.5, multiple channel openings occurred, episodically separated by intervals exhibiting only single openings, resulting in large fluctuations in NP_o throughout the record (Fig. 3E). At pH 8.5, multiple openings were more evenly distributed throughout the record and fluctuations in NP_o were smaller. Thus, at low pH, estimation of channel number was biased and patches at pH 6.5 were likely to have contained more channels than indicated by the maximum number of simultaneously open channels (which measures the minimum number of channels in the patch). Thus, the difference in single-channel open probability between pH 6.5 and 8.5 is likely to have been underestimated in this comparison.

The episodic nature of channel gating at pH 6.5 relative to pH 8.5 may be explained if protonation events that resulted in channel inhibition were long-lived, producing fluctuations in the number of channels available to open. Closed-time distributions (Fig. 3F) from the multichannel current records of Figure 3D indicated the existence of a long-lived closed state at pH 6.5 that was not present at pH 8.5. The closed-time distribution of the pH 6.5 record, excluding events greater than 90 ms, was approximated by the sum of two exponential components: a large proportion of the distribution fit a mean closed time of 8.6 ms and a small proportion fit a mean closed time of 1.0 ms. The long-lived events excluded from the fit were much longer than expected for inclusion in the predominant 8.6 ms kinetic component and too infrequent for estimating a third kinetic component from the record shown. In contrast, the closed-time distribution of the multichannel record at pH 8.5 did not contain such long-lived events; fitting
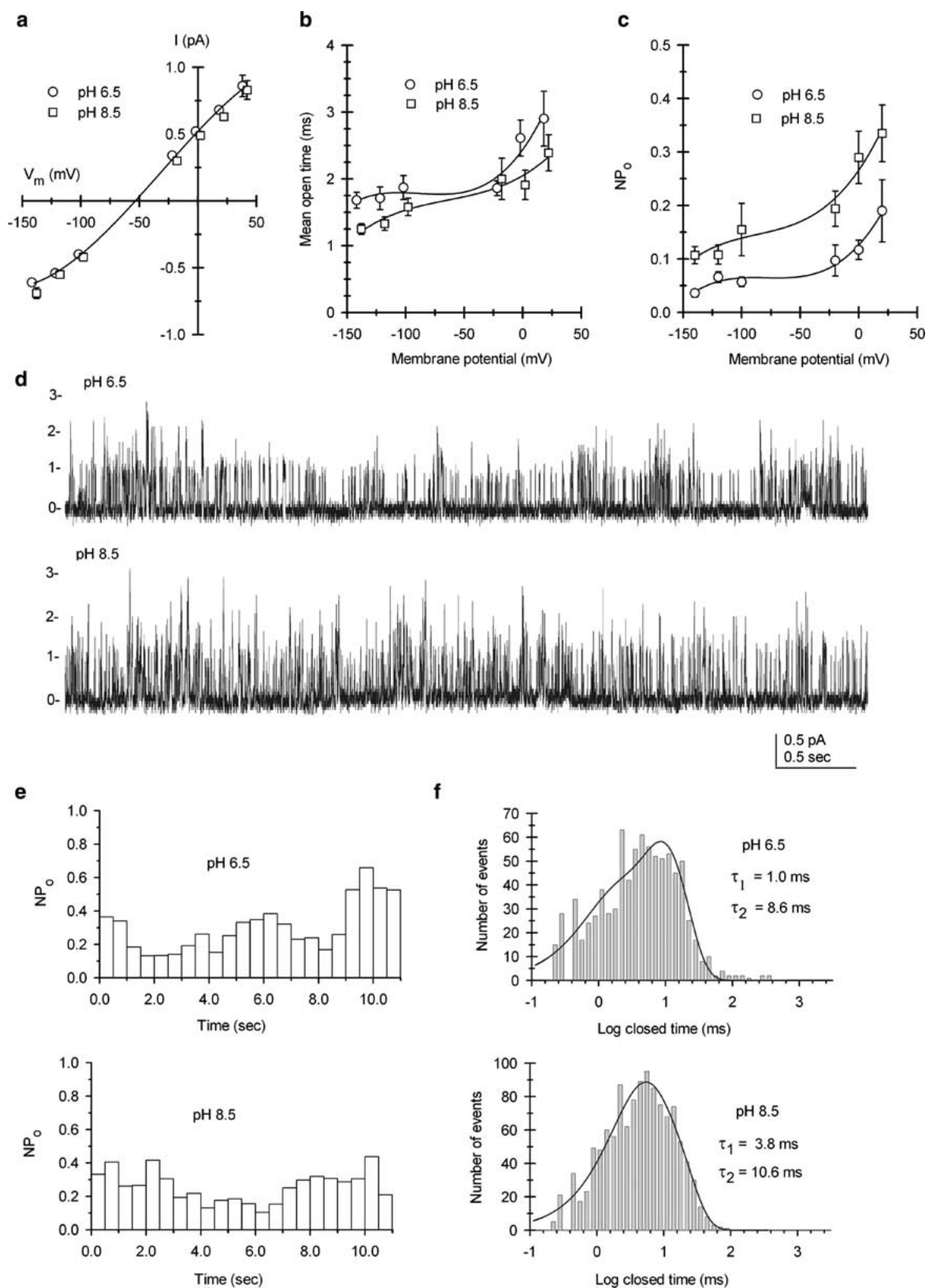
this distribution to two exponential components yielded time constants of 3.8 and 10.6 ms. The short-lived channel closures at both pH 6.5 and 8.5 reflected the tendency of channel to exhibit bursting behavior. Burst-like openings have been observed in cloned TASK-3 channels (Rajan et al., 2002) and native

Fig. 3. Effect of pH on unitary leak channel currents from cell-attached patches. (*A*) Single-channel current voltage relationship is plotted for data obtained using pipette salines buffered to pH 6.5 (*circles*) and pH 8.5 (*squares*). Symbols indicate the mean (± standard error of the mean [SEM]) unitary current amplitude from 10 different patches at pH 8.5 and 12 different patches at pH 6.5; symbols were offset along the voltage axis to clearly reveal means and error bars where they exceeded symbol size. The solid curve represents a third-order linear regression fit of the data. (*B*) Mean open time of unitary events is plotted as a function of membrane potential. Symbols represent the mean ± SEM of data obtained from five to 11 different patches at pH 6.5 (*circles*) and seven to 11 different patches at pH 8.5 (*squares*). The smooth curves represent third-order linear regression fits to the data. (*C*) The voltage dependence of NP_o measured at pH 6.5 (*circles*) and pH 8.5 (*squares*). Symbols represent the mean ± SEM determined from patches at pH 6.5 ($n = 9$), which minimally contained two to five active channels, and patches at pH 8.5 ($n = 9$), which minimally contained three to five active channels, based on the number of simultaneously open channels observed. The smooth curves represent third-order linear regression fits to the data. (*D*) Nonstationary channel gating at pH 6.5 relative to pH 8.5 is illustrated by 5 s of continuous channel activity recorded at 0 mV from cell-attached patches at pH 6.5 (*upper trace*) and pH 8.5 (*lower trace*). Patches appeared to contain similar numbers of channels ($n = 4$), based on the maximum number of simultaneously open channels observed for each patch. Currents were low pass-filtered at 1 kHz. The zero-current level and number of simultaneously open channels are indicated at the left of each trace. (*E*) NP_o values for consecutive 0.5-s intervals from 11 s of continuous recording from the records illustrated in (*D*) at pH 6.5 (*upper graph*) and pH 8.5 (*lower graph*). Time zero corresponds to the beginning of the current traces shown in (*D*). (*F*) Closed-time distributions from the multichannel records shown in (*D*) for pH 6.5 (*upper graph*) and pH 8.5 (*lower graph*). Smooth curves represent fits of the data to the sum of two exponential components, excluding events longer than 90 ms from the fit at pH 6.5.

TASK-like channels from carotid body type 1 cells (Williams & Buckler, 2004). Our measure of the mean lifetime of brief closed-times events (1.0 and 3.8 ms) was substantially longer than the 0.14 ms intraburst mean closed time obtained for native TASK-like channels using 5 kHz low pass filtering (Williams & Buckler, 2004). Our analysis may have missed many short-lived closures due to data filtering. Similarly, mean open times may have been overestimated due to missed channel closings.

LIFETIME OF THE PROTONATED, NONCONDUCTING STATE

Kinetic interpretation of the closed- or blocked-state dwell time distributions from multichannel patch recordings was hindered by nonstationary gating behavior, which contributed to uncertainty in the number of channels in each patch. These problems may be circumvented by confining closed-state distribution analysis to periods in which only a single channel was observed to be active over several seconds of continuous recording. In this regard, the closed-time distribution of pooled data obtained from two such patches at pH 6.5 and a membrane potential of 0 mV approximated the sum of at least three monoexponential components (Fig. 4*A*): a short-lived component of 2.7 ms mean duration, a predominant component of 30.1 ms mean duration and a long-lived component estimated to have a mean duration of 710 ms. Closed-state dwell time distributions from periods containing only one active channel were also obtained from these patches at 20 and 40 mV (*data not shown*). These distributions were similar to the data at 0 mV except that the time constant of the predominant (intermediate) component decreased by nearly 50% between 0 and 40 mV. Unlike the short and intermediate duration events, long-lived events were rarely observed at pH 8.5 and are hypothesized to represent the H^+-induced closed state.

The mean lifetime of the protonation closed state was also determined from macroscopic I_K relaxations in response to a step change in extracellular pH from 6.0 to 8.5, a pH at which reprotonation was expected to be minimal (Fig. 4*B*). Rapid changes in extracellular pH were achieved by opening a superfusion pipette positioned close to the recorded cell; this system achieved complete solution change in approximately 100 ms as estimated from current relaxations in response to a step change in K^+ concentration. As expected for a simple dissociation reaction, I_K relaxations were well described by a monoexponential function, exhibiting a time constant of 660 ± 110 ms (mean ± SD, $n = 4$) (Fig. 4*B*). This response is much slower than the time required to achieve solution exchange and is similar to the long duration closed state observed in single-channel records at pH 6.5. A long dwell time in the protonation-closed state is consistent with the absence of pH effects on macroscopic I_K activation and deactivation kinetics (Fig. 1), which were greater than two orders of magnitude faster.

Conversely, the H^+ association rate was measured from current relaxations in response to a step change from pH 8.5 to 6.0 (Fig. 4*B*). Relaxations exhibited multiexponential kinetics: approximately 50% of the current was rapidly inhibited, exhibiting a time course similar to that required for solution exchange, whereas inhibition of remaining current was slow, requiring several seconds for completion. This pattern of inhibition was observed in all cells examined ($n = 4$), indicating that H^+ inhibition of channel gating is state-dependent.

EFFECT OF Zn^{2+} ON MACROSCOPIC AND UNITARY K^+ CURRENTS

Extracellular Zn^{2+} is reported to selectively inhibit cloned TASK-3 channels relative to TASK-1 and heteromeric TASK-1/TASK-3 channels (Clarke
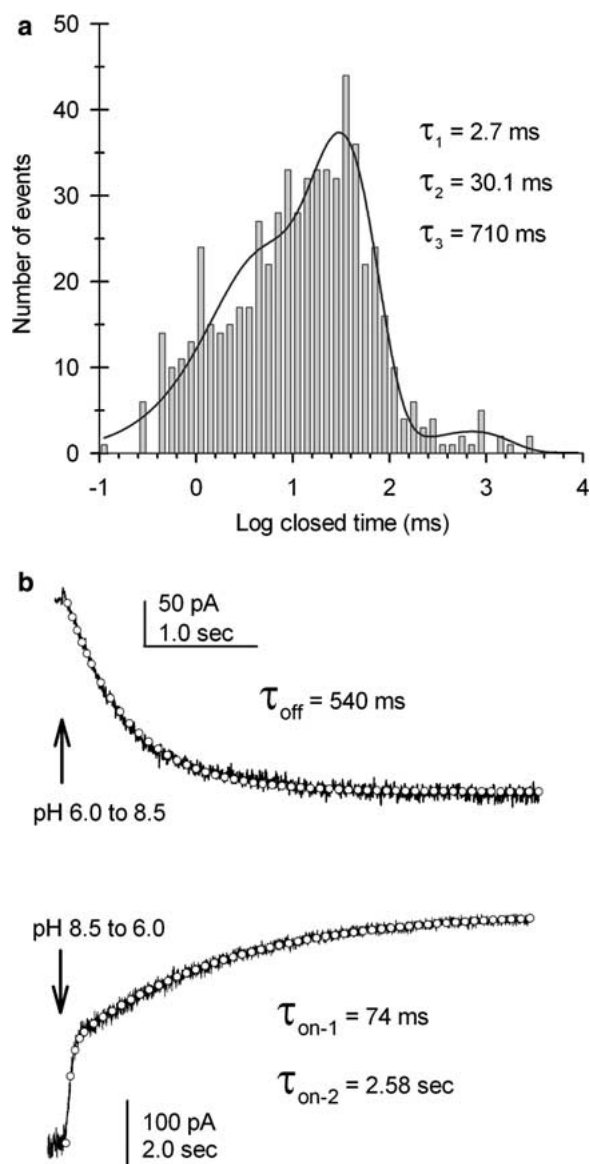
Fig. 4. Lifetime of the protonated-blocked state. (*A*) Closed/blocked-state dwell time distribution at 0 mV. Data were pooled from two cell-attached patches at pH 6.5 exhibiting prolonged periods that appeared to contain a single active channel; each patch contained at least two channels. The smooth curve represents a fit to the sum of three exponential components exhibiting mean durations of 2.7, 30.1 and 710 ms. (*B*) Traces represent I_K relaxations at −100 mV induced by a step change in extracellular pH from 6.0 to 8.5 (*upper trace*) to estimate the mean lifetime of the protonation-blocked state and an oppositely directed step change in pH from 8.5 to 6.0 (*lower trace*) to estimate the rate of H^+-induced channel blockade in a different cell. The I_K relaxation induced by H^+ dissociation is fit to a monoexponential function (*open circles*) exhibiting a time constant of 540 ms. The I_K relaxation induced by protonation is fit to the sum of two exponential functions (*open circles*) exhibiting time constants of 74 ms and 2.58 s. *Arrows* indicate the onset of the pH change. I_K traces were low pass-filtered at 500 Hz.

et al., 2004). The effect of Zn^{2+} on I_K was similar to that of H^+, inducing reversible, concentration-dependent and voltage-independent inhibition without affecting activation or deactivation kinetics (Fig. 5*A*). The E_{rev} of the Zn^{2+}-sensitive current was −60.3 ± 2.1 mV (mean ± SD, $n = 4$), close to the expected E_K of −64 mV (*data not shown*). Zinc inhibition of quasi-steady-state I_K was well described by the Hill equation (equation 1), yielding an IC_{50} of 41.3 μM with a Hill coefficient of 1.26 (Fig. 5*B*). Zn^{2+} also mimicked the effect of H^+ on unitary leak channel currents. Inclusion of 50 μM Zn^{2+} in cell-attached patch pipette saline buffered to pH 8.5 induced the appearance of a long-lived closed state (Fig. 5*C*) without significantly affecting unitary conductance or mean open time (*data not shown*). The closed-time distribution of multichannel current records was approximated by the sum of two monoexponential components (Fig. 5*D*). The short-lived component which measured intraburst closings appeared unaffected by Zn^{2+}; however, the longer-lived component exhibited a time constant of 38.1 ms in the record shown. This was approximately fourfold longer than that typically obtained from control multichannel patches at pH 8.5 (*see* Fig. 3*F*). Induction of a long-lived blocked state is equivalent to reducing the number of channels available to open and is consistent with the absence of Zn^{2+} effects on I_K activation and deactivation rates.

EFFECT OF RUTHENIUM RED

Ruthenium red is a second pharmacological tool selective for TASK-3 over TASK-1 and TASK-1/TASK-3 heteromers (Czirjak & Enyedi, 2002b; Kang et al., 2003). While the concentration dependence of Zn^{2+} inhibition suggests that gK^+ is mediated predominantly by homomeric TASK-3 channels, this conclusion relies on the similarity of rat and human orthologues. Zinc inhibition of AG cell I_K exhibited an IC_{50} of 41 μM, which is near the IC_{50} of 20 μM reported for human TASK-3 (Clarke et al., 2004; Grus et al., 2004) and well below concentrations necessary to substantially inhibit rat and human TASK-1 or human TASK-1/TASK-3 heteromers (Leonoudakis et al., 1998; Clarke et al., 2004). However, cloned rat TASK-1/TASK-3 heteromers appear to be more sensitive to Zn^{2+} than the human orthologue, exhibiting an IC_{50} near 50 μM (D. A. Bayliss, personal communication). On the other hand, ruthenium red selectivity was examined using the rat isoforms and reported to inhibit TASK-3 current by nearly 80% at a concentration of 5 μM while inhibiting TASK-1 or TASK-1/TASK-3 currents by approximately 5% (Czirjak & Enyedi, 2002b; Kang et al., 2003). In AG cells, extracellular application of 5 μM ruthenium red reversibly inhibited quasi-steady-state I_K, by 75.6% ± 5.1% at 0 mV and 78.3% ± 9.9% at −100 mV (mean ± SD, $n = 3$), when measured at the end of 80 ms voltage

a

40 mV

-80 mV

-120 mV

control

25 μM Zn^{2+}

100 μM Zn^{2+}

250 μM Zn^{2+}

500 pA
5 ms

b

c

pH 8.5

pH 8.5 + 50 μM Zn^{2+}

0.5 pA
250 ms

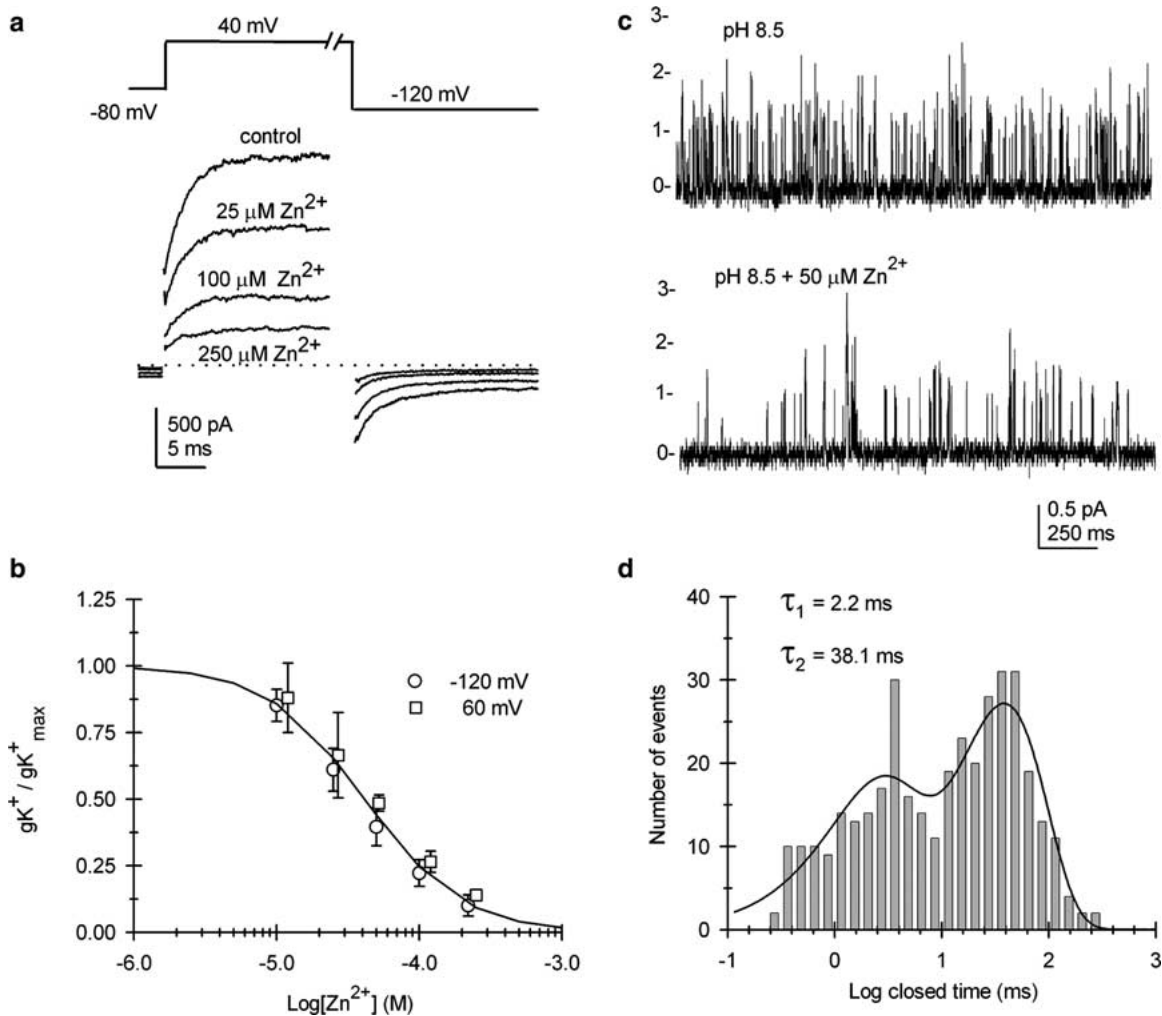**d**

$\tau_1 = 2.2$ ms

$\tau_2 = 38.1$ ms

Fig. 5. Extracellular Zn^{2+} inhibition of macroscopic and unitary K^+ currents. (*A*) Superimposed traces represent I_K from a representative cell evoked by an 80-ms voltage command from -80 to $+40$ mV followed by repolarization to -120 mV in the presence of the indicated Zn^{2+} concentration at an extracellular pH of 7.5. The *uppermost trace* illustrates the voltage paradigm; the *dotted line* indicates the zero-current level. Current records were not leak-subtracted. (*B*) The concentration dependence of Zn^{2+} inhibition of quasi-steady-state gK^+ is plotted for data collected at -100 mV (*circles*) and $+60$ mV (*squares*). The smooth curve represents the best fit of the pooled data to equation 1. Symbols represent means $\pm$ SD ($n = 4$) at each concentration and are offset slightly along the x axis to clearly reveal the data obtained at each voltage.

(*C*) Traces represent leak channel currents recorded at 0 mV and pH 8.5 from separate cell-attached patches; *upper trace* illustrates representative control activity and *lower trace*, a different patch with 50 μM Zn^{2+} added to the pipette saline. The control and Zn^{2+} patches contained at least four and three channels, respectively, based on the number of simultaneously open channels. The zero-current level and number of simultaneously open channels are indicated at the left of each trace. Current records were low pass-filtered at 1,000 Hz. (*D*) The graph illustrates the closed-time distribution of the current record obtained from the patch containing 50 μM Zn^{2+} (*lower trace* of *C*). The smooth curve represents the fit of the data to the sum of two exponential components, exhibiting time constants of 2.2 and 38.1 ms.

commands from a holding potential of -80 mV. Thus, the ruthenium red sensitivity of AG cell I_K approached that of recombinant rat TASK-3, suggesting that TASK-1/TASK-3 heteromers made little contribution to gK^+.

EFFECT OF $M_{G^{2+}}$ ON MACROSCOPIC AND UNITARY K^+ CURRENTS

The divalent ions Mg^{2+} and Ca^{2+} may also be useful for distinguishing currents mediated by different

TASK isoforms. Recombinant TASK-3 and TASK-1/TASK-3 currents are reported to be inhibited by physiological concentrations of Mg^{2+} and Ca^{2+} (Rajan et al., 2000; Kang et al., 2003), whereas TASK-1 is reported to be insensitive (Lopes et al., 2000; Maingret et al., 2002). At physiological concentrations, extracellular Mg^{2+} induced a voltage-dependent block of I_K, inhibiting currents at negative membrane potentials much more so than at positive potentials, without significantly affecting activation or deactivation kinetics (Fig. 6*A*). The E_{rev} of Mg^{2+}-
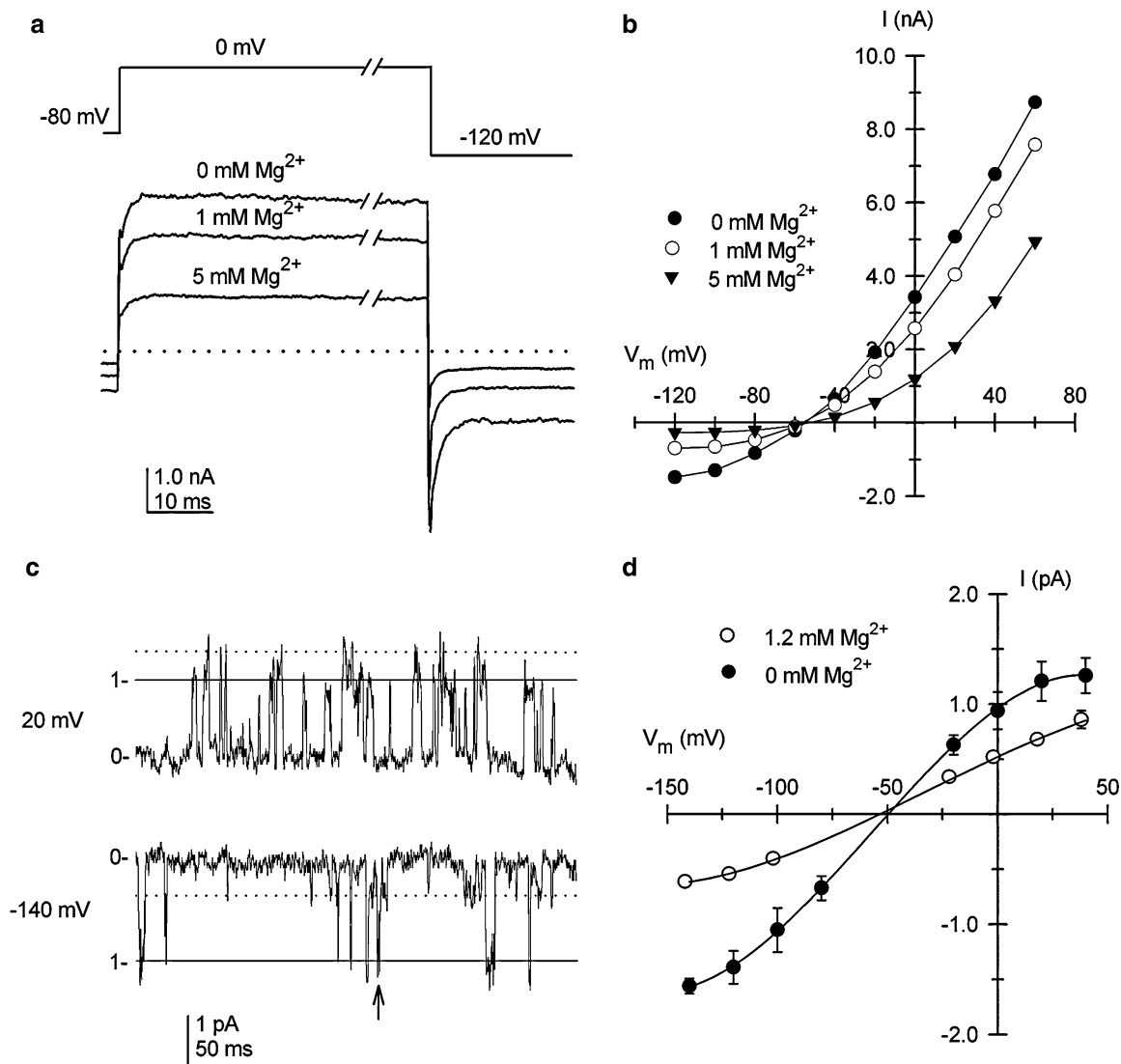
Fig. 6. Extracellular Mg^{2+} block of macroscopic and unitary K^+ currents. (*A*) Superimposed traces represent I_K from a representative cell evoked by an 80-ms depolarizing voltage command from -80 to 0 mV followed by repolarization to -120 mV in nominally divalent cation-free saline (0 mM Mg^{2+}), 1 mM Mg^{2+} and 5 mM Mg^{2+}. Current records were not leak-subtracted; *dashed line* indicates the zero-current level. The *uppermost trace* illustrates the voltage paradigm. (*B*) Effect of Mg^{2+} on the quasi-steady-state current-voltage relationship of the records shown in (*A*). Current was measured at the end of 80-ms voltage commands in nominally divalent cation-free saline (*filled circles*), 1 mM Mg^{2+} (*open circles*) and 5 mM Mg^{2+} (*inverted triangle*). Lines are drawn to connect the symbols. Membrane current was leak-subtracted as described in Methods. (*C*) Traces illustrate unitary leak channel currents

recorded at 20 mV (*upper trace*) and −140 mV (*lower trace*) from a cell-attached patch using nominally divalent cation-free pipette saline buffered to pH 6.5. The zero-current level and predominant unitary current levels are indicated at the left of each trace. *Solid lines* indicate the predominant unitary current level and *dashed lines*, substate current levels (*see* text for discussion). Current records were low pass-filtered at 1,000 Hz. (*D*) Single-channel current voltage relationship obtained from cell-attached patches using nominally divalent cation-free pipette saline (*filled circles*). Symbols represent the mean (± SD) of unitary current amplitudes from three patches. Data obtained in the presence of 1.2 mM Mg^{2+}, pH 6.5, from Figure 3*A* are shown for comparison (*open circles*). Solid curves represent third-order polynomial regression fits of the data.

sensitive current was near E_K as expected for K^+-selective current (Fig. 6*B*). Mg^{2+} inhibited both the instantaneous and time-dependent components of I_K. Similarly, omission of divalent ions from the pipette saline resulted in a voltage-dependent increase in both inward and outward unitary leak currents recorded from cell-attached patches (Fig. 6*C, D*).

Inward unitary conductance increased to nearly 18 pS from approximately 8 pS in 1.2 mM Mg^{2+} (20 mM K^+ pipette saline).

Leak channels exhibited multiple subconductance states that were best illustrated in the large-amplitude unitary currents obtained upon removal of extracellular Mg^{2+} (Fig. 6*C*). Subconductance behavior was

also apparent in the presence of extracellular Mg^{2+} (*see* Fig. 2) but more difficult to document due to the smaller current amplitude. The example record at −140 mV contains both small- and large-amplitude events that did not necessarily summate when simultaneously open (*arrow*), indicating that small-amplitude events represented a subconductance state. This conclusion is also supported by the observation that periods of small- and large-event activity were coincident. Furthermore, the high conductance state itself appeared to represent a subconductance state. This is illustrated in the current record from the same patch at 20 mV. Open channel current was often observed to flicker to higher conductance levels (indicated by the *dashed line*). This flickering often occurred when small-conductance events were infrequent, suggesting that it did not necessarily represent the simultaneous openings of two channels. Subconductance state behavior did not appear related to H^+ or Mg^{2+} inhibition; substate behavior was common at both pH 6.5 and 8.5 and in the presence or absence of Mg^{2+}. Subconductance behavior has also been reported for recombinant TASK-1 and TASK-3 channels (Kim et al., 1999; Lopes et al., 2000; Rajan et al., 2000).

EFFECT OF BUPIVACAINE ON MACROSCOPIC AND SINGLE-CHANNEL K^+ CURRENT

Whereas two-pore domain K^+ channels are characterized by their insensitivity to many traditional K^+ channel blockers, they are inhibited by local anesthetics (Kindler, Yost & Gray, 1999). Of several local anesthetics tested, TASK-1 channels were most sensitive to bupivacaine; TASK-3 channels were reported to exhibit a similar affinity (Meadows & Randall, 2001). Thus, native TASK channel currents are expected to be inhibited by bupivacaine, although bupivacaine has not yet been shown to be useful in discriminating among TASK channel isoforms. The effects of bupivacaine on macroscopic and unitary K^+ currents are shown in Figure 7. Bupivacaine rapidly and reversibly induced a voltage- and concentration-dependent inhibition of I_K and introduced multiple exponential components into the time-dependent components of I_K (Fig. 7A). The concentration dependence of quasi-steady-state current inhibition was well described by the Hill equation (equation 1), yielding IC_{50} values of 116 μM at -100 mV and 28 μM at 40 mV and Hill coefficients of 1 at both potentials (Fig. 7B). Woodhull analysis (equation 2) of voltage-dependent inhibition indicated that bupivacaine traversed 20% of the transmembrane electric field from the cytosolic side of the membrane to reach its binding site. In this regard, inhibition of cloned TASK-1 current with extracellular bupivacaine was attributed to membrane permeation and block from

the cytosolic membrane face (Kindler et al., 1999). Consistent with this interpretation, bath application of 50 μM bupivacaine rapidly and reversibly modified unitary currents recorded from cell-attached patches (Fig. 7C-E). Bupivacaine decreased mean open time (Fig. 7D) and shifted the closed-time distribution of these multichannel records toward shorter-duration events (Fig. 7E) without significantly inhibiting unitary current amplitude. These channel-gating effects were observed at −100 as well as 0 mV (*data not shown*).

EFFECT OF HALOTHANE ON MACROSCOPIC AND UNITARY K^+ CURRENTS

Yet another defining characteristic of TASK channels is their activation by inhalation anesthetics (Patel et al., 1999), although halothane has not been found useful for discriminating between specific TASK channel isoforms (Berg et al., 2004). In AG cells, halothane induced a reversible, concentration-dependent and apparently voltage-independent increase in I_K (Fig. 8A, B). The E_{rev} for halothane-induced current was −64.8 ± 1.3 mV (mean ± SD, $n = 5$) at 1 mM halothane and -65.0 ± 1.2 mV ($n = 5$) at 10 mM halothane, close to the expected E_K of −64 mV. Thus, the large increase in membrane current (Fig. 8B) appeared to be mediated entirely by K^+ channel activation. In this regard, inhibition of TASK channels by lowering extracellular pH to 6.0 completely blocked halothane stimulation of membrane current (*data not shown*), as expected if the increase was mediated by TASK channels (Sirois et al., 2000). The threshold for halothane stimulation appeared to be between 0.1 and 1 mM; membrane-pipette seals often became unstable at halothane concentrations above 10 mM. These concentrations are only approximations in that a vaporizer was not employed to prepare solutions nor was the bath concentration measured directly. In addition to increasing I_K, halothane decreased the time constant for I_K activation (τ_{act}) (Fig. 8C). This effect was most apparent in response to small depolarizing commands. In paired comparisons, halothane decreased τ_{act} in response to voltage commands to 0 mV (from −80 mV holding potential) by 9.0 ± 24.1%, 24.7 ± 26.0% and 46.1 ± 22.2% (mean ± SD) for 1, 5 and 10 mM halothane, respectively. This effect was statistically significant ($P < 0.05$) at 5 and 10 mM halothane. Similar results were obtained for deactivation; however, halothane often introduced multiple exponential components into deactivation kinetics.

Halothane effects on unitary leak channel currents were consistent with effects on I_K. Halothane is reported to increase TASK channel P_o (Patel et al., 1999), and this effect was also observed on leak channel gating. At an extracellular pH of 6.5, bath application of 5 mM halothane increased NP_o
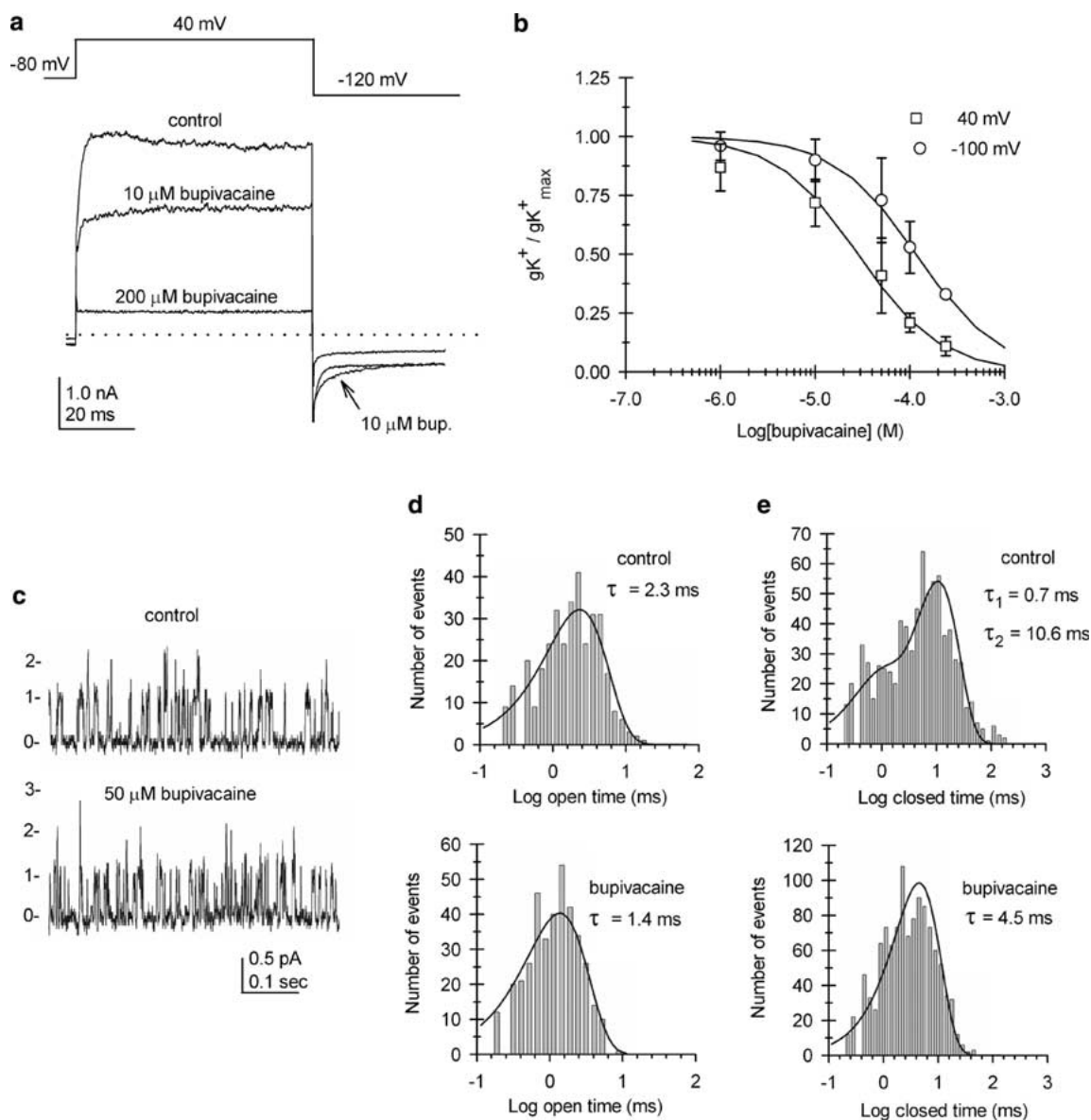
Fig. 7. Bupivacaine block of macroscopic and unitary K⁺ currents. (*A*) Superimposed traces represent I_K from a representative cell evoked by an 80-ms depolarizing voltage command from −80 to +40 mV followed by repolarization to −120 mV in the presence of 0 (control), 10 and 200 μM bupivacaine at pH 7.5. The *uppermost trace* illustrates the voltage paradigm, and the *dotted line* indicates the zero-current level. Current records were not leak-subtracted. (*B*) The concentration dependence of bupivacaine inhibition of quasi-steady-state gK^+ (measured at the end of the voltage command) is plotted for data collected at −100 mV (*circles*) and +40 mV (*squares*). Symbols represent the mean ± SD of three to five separate experiments at each concentration. The smooth curves represent the best fit of each data set to equation 1. (*C*) Traces illustrate representative unitary leak current activity recorded from a cell-attached patch at 0 mV and pH 6.5 before (control, *upper*

trace) and during (*lower trace*) bath application of 50 μM bupivacaine. The zero-current level and number of simultaneously open channels are indicated at the left of each trace. Current records were low pass-filtered at 1,000 Hz. (*D*) Effect of bupivacaine on the open-state dwell time distribution from the recording shown in (*C*). The smooth curves represent the fit of monoexponential functions exhibiting time constants of 2.3 ms for the control (*upper graph*) and 1.4 ms in the presence of 50 μM bupivacaine (*lower graph*). (*E*) Effect of bupivacaine on the closed-time distribution for the patch shown in (*C*). The smooth curves represent the fit of the control data (*upper graph*) to the sum of two exponential functions exhibiting time constants of 0.7 and 10.6 ms. In the presence of 50 μM bupivacaine (*lower graph*), the smooth curve represents the fit of a monoexponential function exhibiting a time constant of 4.5 ms.

by 235% ± 121% (mean ± SD, *n* = 4) in cell-attached patches at 0 mV. In these patches, halothane stimulation did not appear to increase the number of active channels, as estimated from the maximum

number of simultaneously open channels. In other patches (excluded from this comparison), halothane stimulation increased the maximum number of simultaneously open channels by two or more and
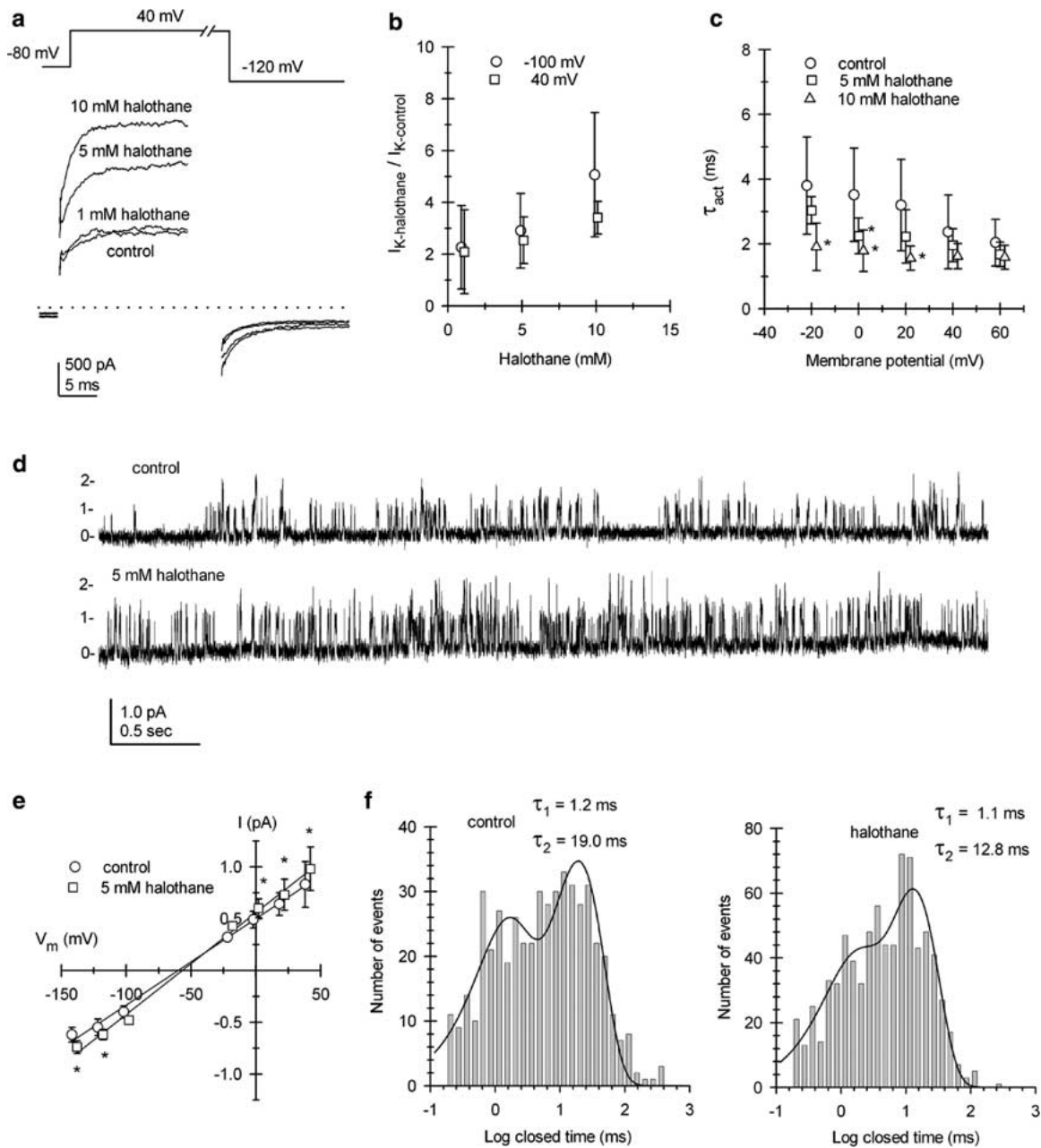
Fig. 8. Halothane stimulation of macroscopic and unitary K^+ currents. (*A*) Superimposed traces represent I_K from a representative cell evoked by an 80-ms depolarizing voltage command from −80 to +40 mV followed by repolarization to −120 mV at pH 7.5 in the presence of 0 (control), 1, 5 and 10 mM halothane. Current records were not leak-subtracted; *dashed line* indicates the zero-current level. The voltage paradigm is illustrated above the current traces. (*B*) Concentration dependence of halothane stimulation of quasi-steady-state I_K measured at the end of 80-ms voltage commands from a holding potential of −80 to −100 mV (*circles*) or +40 mV (*squares*). Each symbol represents the mean ± SD of five to seven separate cells. Symbols are offset along the abscissa to clearly reveal the data. (*C*) Effect of halothane on the time constant of current activation. Each symbol represents the mean ± SD of four to six separate cells: control (*circles*), 5 mM halothane (*squares*) and 10 mM halothane (*triangles*). Symbols are offset along the abscissa to clearly reveal the data. Asterisks indicate a statistically significant ($P < 0.05$) decrease in τ_{act} based on paired comparisons. (*D*) Traces illustrate represen-

tative unitary current activity recorded from a cell-attached patch at 0 mV and pH 6.5 before (control, *upper trace*) and during (*lower trace*) bath application of 5 mM halothane. The zero-current level and number of simultaneously open channels are indicated at the left of each trace. The patch contained a minimum of two active channels. Current records were low pass-filtered at 1,000 Hz. (*E*) Halothane increased single-channel conductance without affecting reversal potential. Symbols indicate means ± SEM of the control data (*circles*) and in the presence of 5 mM halothane (*squares*). Symbols are slightly offset along the x axis to clearly indicate the data. Smooth curves represent linear regression fits to each data set. Asterisks indicate a statistically significant ($P < 0.05$) increase in current based on paired comparisons. (*F*) Effect of halothane on the closed-time distribution obtained from the records shown in (*D*). Smooth curves represent the fit of the data to the sum of two exponential functions, which exhibited time constants of 1.2 and 19.0 ms for the control (*left graph*) and 1.1 and 12.8 ms in the presence of 5 mM halothane (*right graph*).

caused much larger increases in NP_o (*data not shown*). In both cases, the increase in NP_o was not significantly voltage-dependent and similar results were obtained at pH 8.5. Stimulation of P_o was primarily attributable to a decrease in duration of the predominant component of the closed-time distribution. In the multichannel patch recording shown (Fig. 8*D*), this component decreased from 19 to 12.8 ms (Fig. 8*F*). The closed-time distribution of several patches could be approximated by a biexponential distribution similar to that shown in Figure 8*F*. In these patches, halothane stimulation decreased the predominant (slower) component to $44\% \pm 22\%$ (mean $\pm$ SD, $n = 4$) of the control value at 0 mV; a similar decrease was observed at negative membrane potentials (*data not shown*). As described above and reported previously for TASK-1 (Sirois et al., 2000), channels inhibited by protonation cannot be activated by halothane. In this regard, it is of interest that long closed-time events (>100 ms) recorded at pH 6.5 persisted in the presence of halothane, although less frequently than in the control (Fig. 8*F*). Halothane was not observed to significantly affect mean open times measured at hyperpolarized potentials (-100 mV or less) (*data not shown*). At depolarized potentials, the large number of simultaneous channel openings during halothane stimulation biased measurement of mean open time toward shorter durations even at pH 6.5. However, the records shown in Figure 8*D* at 0 mV contained relatively few double openings and the mean open times from these data were 2.5 and 2.4 ms for the control and in the presence of halothane, respectively. Halothane also induced a small but statistically significant increase in single-channel conductance without affecting E_{rev} (Fig. 8*E*).

Halothane stimulation of recombinant TASK channels is also observed in isolated membrane patches (Patel et al., 1999), indicating a direct effect on channel protein. Indeed, site-directed mutagenesis has identified a six-amino acid sequence near the interface of the fourth transmembrane domain and cytoplasmic C-terminal tail required for halothane stimulation of channel activity (Patel et al., 1999; Talley & Bayliss, 2002). Similarly, halothane effects on leak channels were also observed in isolated inside-out patches: increasing NP_o, decreasing the time constant of the predominant component of the closed-time distribution and increasing unitary current amplitude (*data not shown*).

Discussion

TASK-3-like Channels Mediate Glomerulosa Cell gK^+

The present study demonstrates that rat AG cell gK^+ is mediated almost entirely by TASK channels whose biophysical and pharmacological properties most closely resemble those of recombinant TASK-3. Macroscopic I_K was inhibited by several treatments known to inhibit recombinant TASK channels (extracellular H^+, Zn^{2+}, Mg^{2+}, ruthenium red and bupivacaine) and activated by the inhalation anesthetic halothane. Furthermore, treatment effects on unitary leak channel currents were consistent with effects on the macroscopic current. Our previous studies had suggested that AG cell gK^+ was mediated by two K^+ channel types, the weakly voltage-dependent leak channel and a strongly voltage-dependent channel, which could not be distinguished at the single-channel level (Lotshaw, 1997a). This interpretation was based on predictions of macroscopic I_K behavior from extrapolations of leak channel biophysical properties and selective inhibition of depolarization-activated, time-dependent I_K by quinidine. The present study has demonstrated that leak channels are predominantly responsible for mediating both voltage-independent and voltage-dependent components of gK^+. Although rat AG cells are reported to express both TASK-1 and TASK-3 genes, neither TASK-1 nor heteromeric TASK-1/TASK-3 channels appeared to contribute significantly to gK^+. This conclusion is supported by the sensitivity of gK^+ to Zn^{2+} and ruthenium red. The TASK-3 isoform exhibits the highest sensitivity to these drugs, and Zn^{2+} inhibition of AG cell gK^+ approached the sensitivity of recombinant rat and human TASK-3 (Clarke et al., 2004; Grus et al., 2004; D. A. Bayliss, personal communication). This result should exclude homomeric TASK-1 channels as a significant contributor to gK^+ but not TASK-1/TASK-3 heteromers, which appear to be substantially more Zn^{2+}-sensitive in the rat than the human orthologue (D. A. Bayliss, personal communication). The sensitivity of the AG cell gK^+ to a low concentration of ruthenium red indicated that TASK-1/TASK-3 heteromers make little or no contribution, in agreement with results obtained from ruthenium red inhibition of I_K induced by rat AG cell mRNA expression in *Xenopus* oocytes (Czirjak & Enyedi, 2002a). Additional evidence for the absence of homomeric TASK-1 channels was provided by our inability to identify TASK-1-like channels in cell-attached patches. Although small-amplitude unitary currents were commonly observed, their characteristics were inconsistent with TASK-1. Instead, these events appeared to represent subconductance states of the 12 pS leak channel: small-amplitude events occurred only coincidently with the 12-pS currents, they were not selectively eliminated from cell-attached patches at pH 6.5 and their amplitude was increased by omission of extracellular Mg^{2+}. An additional criterion considered for identifying the presence of TASK-1 was the human TASK-1-selective inhibitor anandamide and its more stable

analogue methanandamide (Maingret et al., 2001). In the rat, however, TASK-1, TASK-3 and TASK-1/TASK-3 heteromers were reported to exhibit similar sensitivities to both anandamide and methanandamide (Berg et al., 2004). Inhibition similar to that reported by Berg et al. (2004) was obtained in the AG cell: 1 μM anandamide inhibited I_K by approximately 15% (*data not shown*).

Glomerulosa cell leak channel characteristics departed from those of recombinant TASK-3 in what is often regarded as a hallmark for TASK isoform identification, pH sensitivity. Hill equation fits yielded an IC_{50} of pH 7.25 and a Hill coefficient of 0.75 for H^+ inhibition of AG cell gK^+ compared to an IC_{50} near pH 6.8 and a Hill coefficient near 2 for recombinant rat TASK-3 (Kim et al., 2000; Berg et al., 2004). This result indicates that either native TASK-3 channels are subject to modifications that alter pH sensitivity or the IC_{50} for H^+ inhibition represented the response of multiple TASK isoforms. As noted in the preceding paragraph, there is little experimental support for the latter interpretation. Although a small contribution to gK^+ from TASK-1/TASK-3 heteromers could not be excluded, it would seem unlikely to produce such a shift in pH sensitivity. Assuming that gK^+ is mediated predominantly by native TASK-3 channels, the use of relative H^+ sensitivity may be a poor criterion for identifying TASK isoforms comprising native channels. Site-directed mutagenesis of TASK genes has demonstrated that a conserved histidine (H98) within the first pore domain is the primary determinant of TASK channel pH sensitivity (Kim et al., 2000; Rajan et al., 2000; Lopes, Zilberberg & Goldstein, 2001; Morton et al., 2003) and the amino acid sequences neighboring H98 are highly conserved in TASK-1 and TASK-3. Nevertheless, the IC_{50} and Hill coefficients reported for H^+ block of cloned TASK-1, TASK-3 and TASK-1/TASK-3 differ substantially. Large differences also appear between species orthologues, as in rat and guinea pig TASK-3, which exhibited IC_{50} values of pH 6.7 and 6.0 and Hill coefficients of 2.0 and 0.5, respectively (Kim et al., 2000; Rajan et al., 2000). The extent to which these differences reflect methodologies is unclear, but sensitivity to H^+ inhibition is also strongly affected by factors such as permeant ion concentration (Lopes et al., 2001; Morton et al., 2003).

NATIVE TASK CHANNEL BIOPHYSICAL AND PHARMACOLOGICAL PROPERTIES: ION CONDUCTANCE AND VOLTAGE DEPENDENCE

Under a physiological K^+ concentration gradient, steady-state macroscopic currents mediated by recombinant TASK-1 and TASK-3 are often described as open rectifiers, obeying Goldman-Hodgkin-Katz (GHK) constant field equation predictions (Lesage & Lazdunski, 2000; Goldstein et al., 2001; Bayliss et al., 2003). However, characterization of TASK channels as simple open rectifiers is misleading. Recombinant and AG cell TASK currents exhibit both instantaneous and time-dependent changes in response to voltage commands (Lopes et al., 2000; Rajan et al., 2000; Meadows & Randall, 2001; Clarke et al., 2004). Instantaneous current jumps reflect changes in K^+ flux through channels open at the onset of the voltage jump; time-dependent changes reflect voltage-dependent modulation of gating or channel block. Steady-state AG cell I_K approximated GHK predictions for open rectification over a narrow range of negative potentials; however, extension of the voltage range resulted in significant deviations from GHK predictions (*data not shown*). Deviation from GHK can be attributed to ion conduction characteristics, voltage-dependent block by divalent ions and voltage-dependent modulation of gating. Even if only instantaneous current responses to voltage commands are considered, TASK channels are thought to be multi-ion pores (Ilan & Goldstein, 2001) and ion interactions within the pore invalidate the assumption of independence embodied in the GHK equation. Furthermore, depolarizing and hyperpolarizing voltage commands are expected to result in nearly instantaneous relief or strengthening, respectively, of Mg^{2+} and Ca^{2+} block, inducing further deviation from GHK predictions. More problematic for fitting steady-state current to GHK predictions is voltage-dependent modulation of gating. Thus, over an extended range of potentials, neither AG cell leak channels nor cloned TASK channels are expected to obey GHK predictions for open rectification at either the macroscopic or single-channel levels.

Glomerulosa cell leak channel biophysical properties were most similar to those of recombinant TASK-3 channels, exhibiting noninactivating gating, weakly voltage-dependent low open probabilities and brief mean open times (Kim et al., 2000; Rajan et al., 2000; Han et al., 2002). Rat TASK-3 channels are reported to exhibit an inward conductance of 27 pS in symmetrical high-K^+ solutions and 2 mM extracellular Mg^{2+} (Kim et al., 2000). Under these ionic conditions, AG cell leak channels exhibited an inward slope conductance of 24 pS (Lotshaw, 1997a). Leak channel inward conductance increased to >70 pS when Mg^{2+} was omitted from this high-K^+ pipette saline (*data not shown*), similar to the effect on TASK-3 (Rajan et al., 2002). Macroscopic AG cell I_K exhibited weakly voltage-dependent activation kinetics similar to those reported for cloned guinea pig TASK-3 (Rajan et al., 2000), although substantially faster than those reported for human TASK-3 (Meadows & Randall, 2001). The voltage dependence of leak channel open probability was similar to that of the macroscopic current. Increased open probability

was attributable to both an increase in mean open time and a decrease in the predominant component of closed-state dwell time distribution (obtained from multichannel records, *data not shown*).

H$^+$ Inhibition

Proton inhibition of recombinant TASK channel current is predominantly attributed to a decrease in open probability (Kim et al., 1999, 2000), although inhibition of single-channel conductance has also been reported (Kim et al., 2000; Rajan et al., 2000; Han et al., 2002; Kang et al., 2003). In the present study, lowering pH decreased leak channel NP$_o$ values without affecting mean open time or unitary conductance. Inhibition correlated with the appearance of a long-duration closed state postulated to represent the protonation-induced closed state. Recovery of I$_K$ from H$^+$ inhibition followed a slow monoexponential process, exhibiting a time constant similar to that of the long closed state observed at pH 6.5. These results suggest that protonation promotes channel entry into a long-lived closed state, a phenomenon also observed in other ion channel classes including inwardly rectifying K$^+$ channels (Yang et al., 2000) and *N*-methyl-D-aspartate receptors (Traynelis & Cull-Candy, 1991). The lifetime of this state is several orders of magnitude longer than the 60 µs lifetime of protonated glutamate residues that block the L-type Ca^{2+} channel pore (Prod'ham, Pietrobon & Hess, 1987; Chen, Bezprozvanny & Tsien, 1996). Given an IC$_{50}$ of 56 nM for H$^+$ inhibition of AG cell leak channels and assuming an association rate constant similar to that determined by Prod'ham et al. (1987), we might expect the lifetime of the protonated state to be approximately 45 µs. A simple first-order rate constant for H$^+$ inhibition of I$_K$ is unlikely because, in response to the step change in pH, I$_K$ inhibition exhibited complex kinetics. Thus, either protonation, entry into the long-lived closed state or both are state-dependent. Nevertheless, the long lifetime of this closed state greatly exceeds that expected of any amino acid R group protonation reaction, indicating that protonation promotes a conformational change that stabilizes this closed state.

Zn^{2+} Inhibition

Although cloned rat TASK-3 channels were initially described as insensitive to Zn^{2+} (Kim et al., 2000), a subsequent study revealed that Zn^{2+} is selective for TASK-3 relative to other TASK isoforms (Clarke et al., 2004). Zinc binding to human TASK-3 involves a glutamate at position 70 (E70) and a histidine at position 98 (H98), which are located immediately preceding and within the first pore domain, respectively (Clarke et al., 2004). The lower sensitivity of TASK-1 and TASK-1/TASK-3 heteromers to Zn^{2+} (and ruthenium red) is attributed to substitution of lysine for glutamate at position 70 in TASK-1 (Czirjak & Enyedi, 2003; Clarke et al., 2004). Because H98 is involved in mediating both Zn^{2+} and H$^+$ inhibition of TASK-3, it is perhaps not surprising that these inhibitors exerted similar effects on AG cell macroscopic and unitary currents. Both treatments caused a voltage-independent inhibition of I$_K$ without affecting activation or deactivation kinetics and introduced a long-lived closed state without affecting mean open time or unitary conductance. Thus, like H$^+$, Zn^{2+} inhibited I$_K$ by reducing the number of channels available for opening.

Bupivacaine Inhibition

Bupivacaine effects on AG cell gK$^+$ were similar to those reported for recombinant rat TASK-1 and TASK-3 currents. TASK-1 inhibition was weakly voltage-dependent, with IC$_{50}$ values of 41 and 68 µM being reported for depolarized potentials (Leonoudakis et al., 1998; Kindler et al., 1999). TASK-3 current is approximately 50% inhibited at 100 µM bupivacaine (Meadows & Randall, 2001; Han et al., 2002). The voltage dependence of TASK-1 inhibition suggested that channel block is mediated by the electrically charged form of bupivacaine approaching its binding site from the cytosol (Kindler et al., 1999). The voltage dependence of AG cell I$_K$ inhibition was similar: in both studies, bupivacaine appeared to bind a site located approximately 20% of the distance through the transmembrane electric field from the cytosolic face. Bupivacaine effects on AG cell leak channel mean open time and closed time distribution indicate this blocker acted by selectively binding the open state and that channel closure required blocker dissociation.

Halothane Activation

Halothane effects on I$_K$ and unitary leak channels were similar to those of recombinant TASK channels (Patel et al., 1999; Meadows & Randall, 2001; Talley & Bayliss, 2002; Berg et al., 2004); however, the extent of the stimulation often greatly exceeded that reported for recombinant channels. This difference may be partially explained by the tendency of the AG cell leak channels to enter a "sleepy state," in which channels did not open prior to halothane stimulation. The existence of a sleepy state was suggested by the observation in cell-attached patches that the maximum number of simultaneously open channels increased substantially in some patches during halothane stimulation. This effect occurred in approximately 25% of patches at both pH 6.5 and 8.5 and could not be attributed simply to the increase in open probability (*data not shown*). This phenomenon is

reminiscent of TREK channels, which may exhibit little or no basal activity prior to stimulation with inhalation anesthetics, membrane stretch or a variety of other treatments (Franks & Honoré, 2004). Although halothane caused a small increase in unitary leak channel amplitude in the AG cell patches, it was not observed to induce the much larger unitary currents characteristic of TREK-1 or TREK-2 (Patel et al., 1998; Lesage et al., 2000). Thus, sleepy channels would not contribute to control current but would become active in the presence of halothane, effectively increasing the number of active channels in addition to increasing open probability. The basis of leak channel "sleep" is unknown, as is the mechanism by which halothane might awaken sleepy channels. Halothane stimulation of recombinant TASK-1 macroscopic current is attributed to an increase in open probability (Patel et al., 1999). Results from the present study indicated that halothane acts primarily by increasing the rate constant for channel opening without affecting the closing rate constant.

DISCREPANCIES BETWEEN NATIVE CHANNEL AND RECOMBINANT CHANNEL PROPERTIES

Investigations of native channels have largely focused on channel identification, correlating native channel properties with those of recombinant channels. Interpretation of the results obtained from many cell types has been complicated by the apparent expression of multiple channel isoforms and subfamilies exhibiting overlapping pharmacological and biophysical properties (Han et al., 2002; Kang et al., 2003; Berg et al., 2004; Williams & Buckler, 2004). The least ambiguous data have come from cell types which appear to express a single type of leak channel current, although the protein subunit composition of even these channels has yet to be determined. Results of the present study suggest that native TASK-3 channels can exhibit a substantial departure in pH sensitivity from that of recombinant TASK-3 channels. A second cell type reported to express a single type of leak K^+ channel is the rat type-I carotid body cell (Buckler, Williams & Honore, 2000; Williams & Buckler, 2004). The properties of this channel closely resembled those of recombinant TASK-1, with the interesting exception that the native channel was blocked by extracellular Mg^{2+} whereas recombinant TASK-1 channels are reported to be insensitive to extracellular Mg^{2+} (Lopes et al., 2000; Maingret et al., 2002). Whether differences between native channels and their presumed recombinant counterparts are attributable to posttranslational modifications or auxiliary subunits remains to be determined.

References

Ashmole, I., Goodwin, P.A., Stanfield, P.R. 2001. TASK-5, a novel member of the tandem pore K^+ channel family. *Pflüegers Arch.* **44:**828–833

Bayliss, D.A., Sirois, J.E., Talley, E.M. 2003. The TASK family: Two-pore domain background K^+ channels. *Mol. Interv.* **3:**205–219

Berg, A.P., Talley, E.M., Manger, J.P., Bayliss, D.A. 2004. Motoneurons express heteromeric TWIK-related acid-sensitive K^+ (TASK) channels containing TASK-1 (KCNK3) and TASK-3 (KCNK9) subunits. *J. Neurosci.* **24:**6693–6702

Bockenhauer, D., Zilberberg, N., Goldstein, S.A.N. 2001. KCNK2: Reversible conversion of a hippocampal potassium leak into a voltage-dependent channel. *Nat. Neurosci.* **4:**486–491

Buckler, K.J., Williams, B.A., Honore, E. 2000. An oxygen-, acid- and anaesthetic-sensitive TASK-like background potassium channel in rat arterial chemoreceptor cells. *J. Physiol.* **525:**135–142

Chen, X.-H., Bezprozvanny, I., Tsien, R.W. 1996. Molecular basis of proton block of L-type Ca^{2+} channels. *J. Gen. Physiol.* **108:**363–374

Clarke, E.C., Veale, E.L., Green, P.J., Meadows, H.J., Mathie, A. 2004. Selective block of the human 2-P domain potassium channel, TASK-3, and native leak potassium current, IK_{SO}, by zinc. *J. Physiol.* **560:**51–62

Czirjak, G., Enyedi, P. 2002a. TASK-3 dominates the background potassium conductance in rat adrenal glomerulosa cells. *Mol. Endocrinol.* **16:**621–629

Czirjak, G., Enyedi, P. 2002b. Formation of functional heterodimers between the TASK-1 and TASK-3 two-pore domain potassium channel subunits. *J. Biol. Chem.* **277:**5426–5432

Czirjak, G., Enyedi, P. 2003. Ruthenium red inhibits TASK-3 potassium channel by interconnecting glutamate 70 of the two subunits. *Mol. Pharmacol.* **63:**646–652

Czirjak, G., Fischer, T., Spat, A., Lesage, F., Enyedi, P. 2000. TASK (TWIK-related acid-sensitive K^+ channel) is expressed in glomerulosa cells of rat adrenal cortex and inhibited by angiotensin II. *Mol. Endocrinol.* **14:**863–874

Duprat, F., Lesage, F., Fink, M., Reyes, R., Heurteaux, C., Lazdunski, M. 1997. TASK, a human background K^+ channel to sense external pH variations near physiological pH. *EMBO J.* **16:**5464–5471

Enyeart, J.A., Danthi, S., Enyeart, J.J. 2004. TREK-1 K^+ channels couple angiotensin II receptors to membrane depolarization and aldosterone secretion in bovine adrenal glomerulosa cells. *Am. J. Physiol. Endocrinol. Metab.* **287:**1154–1165

Franks, N.P., Honoré, E. 2004. The TREK K_{2P} channels and their role in general anesthesia and neuroprotection. *Trends Pharmacol. Sci.* **25:**601–608

Goldstein, S.A.N., Bockenhauer, D., O'Kelly, I., Zilberberg, N. 2001. Potassium leak channels and the KCNK family of two-P-domain subunits. *Nat. Rev. Neurosci.* **2:**175–184

Grus, M., Mathie, A., Lieb, W.R., Franks, N.P. 2004. The two-pore-domain K^+ channels TREK-1 and TASK-3 are differentially modulated by copper and zinc. *Mol. Pharmacol.* **66:**530–537

Han, J., Truell, J., Gnatenco, C., Kim, D. 2002. Characterization of four types of background potassium channels in rat cerebellar granule neurons. *J. Physiol.* **542:**431–444

Horn, R. 1991. Estimating the number of channels in patch recordings. *Biophys. J.* **60:**433–439

Ilan, N., Goldstein, S.A.N. 2001. KCNK0: Single, cloned potassium leak channels are multi-ion pores. *Biophys. J.* **80:**241–253

Kang, D., Han, J., Talley, E.M., Bayliss, D.A., Kim, D. 2003. Functional expression of TASK-1/TASK-3 heteromers in cerebellar granule cells. *J. Physiol.* **554:**64–77

Karschin, C., Wischmeyer, E., Preisig-Muller, R., et al. 2001. Expression pattern in brain of TASK-1, TASK-3 and a tandem pore domain K$^+$ channel subunit, TASK-5, associated with the central auditory nervous system. *Mol. Cell. Neurosci.* **18:**632–648

Ketchum, K.A., Joiner, W.J., Sellers, A.J., Kaczmarek, L.K., Goldstein, S.A.N. 1995. A new family of outwardly rectifying potassium channel proteins with two pore domains in tandem. *Nature* **376:**690–695

Kim, Y., Bang, H., Kim, D. 1999. TBAK-1 and TASK-1, two-pore K$^+$ channel subunits: Kinetic properties and expression in rat heart. *Am. J. Physiol. Heart Circ. Physiol.* **277:**1669–1678

Kim, Y., Bang, H., Kim, D. 2000. TASK-3, a new member of the tandem pore K$^+$ channel family. *J. Biol. Chem.* **275:**9340–9347

Kim, D., Gnatenco, C. 2001. TASK-5, a new member of the tandem-pore K$^+$ channel family. *Biochem. Biophys. Res. Commun.* **284:**923–930

Kindler, C.H., Yost, C.S., Gray, A.T. 1999. Local anesthetic inhibition of baseline potassium channels with two pore domains in tandem. *Anesthesiology* **90:**1092–1102

Lauritzen, I., Zanzouri, M., Honore, E., Duprat, F., Ehrengruber, M.U., Lazdunski, M., Patel, A.J. 2003. K$^+$-dependent cerebellar granule neuron apoptosis. *J. Biol. Chem.* **278:**32068–32076

Leonoudakis, D., Gray, A.T., Winegar, B.D. , et al. 1998. An open rectifier potassium channel with two pore domains in tandem cloned from rat cerebellum. *J. Neurosci.* **18:**868–877

Lesage, F., Lazdunski, M. 2000. Molecular and functional properties of two-pore-domain potassium channels. *Am. J. Physiol. Renal Physiol.* **279:**793–801

Lesage, F., Terrenoire, C., Romey, G., Lazdunski, M. 2000. Human TREK2, a 2P domain mechano-sensitive K$^+$ channels with multiple regulations by polyunsaturated fatty acids, lysophospholipids, and G$_s$, G$_i$, and G$_q$ protein-coupled receptors. *J. Biol. Chem.* **275:**28398–28405

Lopes, C.M.B., Gallagher, P.G., Buck, M.E., Butler, M.H., Goldstein, S.A.N. 2000. Proton block and voltage gating are potassium-dependent in the cardiac leak channel Kcnk3. *J. Biol. Chem.* **275:**16969–16978

Lopes, C.M.B., Zilberberg, N., Goldstein, S.A.N. 2001. Block of Kcnk3 by protons: Evidence that 2-P-domain potassium channel subunits function as homodimers. *J. Biol. Chem.* **276:**24449–24452

Lotshaw, D.P. 1997a. Characterization of angiotensin II-regulated K$^+$ conductance in rat adrenal glomerulosa cells. *J. Membr. Biol.* **156:**261–277

Lotshaw, D.P. 1997b. Effects of K$^+$ channel blockers on K$^+$ channels, membrane potential, and aldosterone secretion in rat adrenal zona glomerulosa cells. *Endocrinology* **138:**4167–4175

Lotshaw, D.P. 2001. Role of membrane depolarization and T-type Ca^{2+} channels in angiotensin II and K$^+$ stimulated aldosterone secretion. *Mol. Cell. Endocrinol.* **175:**157–171

Maingret, F., Honore, E., Lazdunski, M., Patel, A.J. 2002. Molecular basis of voltage-dependent gating of TREK-1, a mechano-sensitive K$^+$ channel. *Biochem. Biophys. Res. Commun.* **292:**339–346

Maingret, F., Patel, A.J., Lazdunski, M., Honore, E. 2001. The endocannabinoid anandamide is a direct and selective blocker of the background K$^+$ channel TASK-1. *EMBO J.* **20:**47–54

Meadows, H.J., Randall, A.D. 2001. Functional characterization of human TASK-3, an acid-sensitive two-pore domain potassium channel. *Neuropharmacology* **40:**551–559

Medhurst, A.D., Rennie, G., Chapman, C.G. , et al. 2001. Distribution analysis of human two pore domain potassium channels in tissues of the central nervous system and periphery. *Mol. Brain Res.* **86:**101–114

Morton, M.J., O'Connell, A.D., Sivaprasadarao, A., Hunter, M. 2003. Determinants of pH sensing in the two-pore domain K$^+$ channels TASK-1 and -2. *Pfluegers Arch.* **445:**577–583

Patel, A.J., Honore, E., Lesage, F., Fink, M., Romey, G., Lazdunski, M. 1999. Inhalation anesthetics activate two-pore domain background K$^+$ channels. *Nat. Neurosci.* **2:**422–426

Patel, A.J., Honore, E., Maingret, F., Lesage, F., Fink, M., Duprat, F., Lazdunski, M. 1998. A mammalian two pore domain mechano-gated S-like K$^+$ channel. *EMBO J.* **17:**4283–4290

Plant, L.D., Rajan, S., Goldstein, S.A.N. 2005. K2P channels and their protein partners. *Curr. Opin. Neurobiol.* **15:**326–333

Prod'ham, B., Pietrobon, D., Hess, P. 1987. Direct measurement of proton transfer rates to a group controlling the dihydropyridine-sensitive Ca^{2+} channel. *Nature* **329:**243–246

Rajan, S., Plant, L.D., Rabin, M.L., Butler, M.H., Goldstein, S.A.N. 2005. Sumoylation silences the plasma membrane leak K$^+$ channel K2P1. *Cell* **121:**37–47

Rajan, S., Preisig-Muller, R., Wischmeyer, E., Nehring, R., Hanley, P.J., Renigunta, V., Musset, B., Schlichthörl, G., Derst, C., Karschin, A., Daut, J. 2002. Interaction with 14-3-3 proteins promotes functional expression of the potassium channels TASK-1 and TASK-3. *J. Physiol.* **545:**13–26

Rajan, S., Wischmeyer, E., Liu, G.-X., Presig-Muller, R., Daut, J., Karschin, A., Derst, C. 2000. TASK-3, a novel tandem pore domain acid-sensitive K$^+$ channel. *J. Biol. Chem.* **275:**16650–16657

Sirois, J.E., Lei, Q., Talley, E.M., Lynch, C. III, Bayliss, D.A. 2000. The TASK-1 two-pore domain K$^+$ channel is a molecular substrate for neuronal effects of inhalation anesthetics. *J. Neurosci.* **20:**6347–6354

Spät, A., Hunyady, L. 2004. Control of aldosterone secretion: A model for convergence in cellular signaling pathways. *Physiol. Rev.* **84:**489–539

Talley, E.M., Bayliss, D.A. 2002. Modulation of TASK-1 (Kcnk3) and TASK-3 (Kcnk9) potassium channels. *J. Biol. Chem.* **277:**17733–17742

Talley, E.M., Lei, Q., Sirois, J.E., Bayliss, D.A. 2000. TASK-1, a two-pore domain K$^+$ channel, is modulated by multiple neurotransmitter in motoneurons. *Neuron* **25:**399–410

Talley, E.M., Solorzano, G., Lei, Q., Kim, D., Bayliss, D.A. 2001. CNS distribution of members of the two-pore-domain (KCNK) potassium channel family. *J. Neurosci.* **21:**7491–7505

Traynelis, S.F., Cull-Candy, S.G. 1991. Pharmacological properties and H$^+$ sensitivity of excitatory amino acid receptor channels in rat cerebellar granule neurons. *J. Physiol.* **433:**727–763

Williams, B.A., Buckler, K.J. 2004. Biophysical properties and metabolic regulation of a TASK-like potassium channel in rat carotid body type 1 cells. *Am. J. Physiol. Lung Cell. Mol. Physiol.* **286:**L221–L230

Woodhull, A.M. 1973. Ionic blockage of sodium channels in nerve. *J. Gen. Physiol.* **61:**687–708

Yang, Z., Xu, H., Cui, N., Qu, Z., Chanchevalap, S., Shen, W., Jiang, C. 2000. Biophysical and molecular mechanisms underlying the modulation of heteromeric Kir4.1-Kir5.1 channels by CO$_2$ and pH. *J. Gen. Physiol.* **116:**33–45